



**GE Research &  
Development Center**

**Final Report: September 1994–November 1997**

**Contract F49620-94-C-0020**

**DISTRIBUTION STATEMENT A**

**Approved for public release  
Distribution Unlimited**

# ***Turbulence-Chemistry Models in Highly Strained Non-Premixed Flames***

***Submitted to***

**U.S. Air Force Office of Scientific Research  
Bolling Air Force Base, DC 20332**

***Prepared by***

**S.M. Correa and I.Z. Hu  
Mechanical Systems Laboratory  
GE Corporate Research and Development  
Niskayuna, New York 12309**

**January 30, 1998**

# REPORT DOCUMENTATION PAGE

Form Approved  
OMB No. 0704-0188

Public reporting burden for this collection of information is estimated to average 1 hour per response, including the time for reviewing instructions, searching existing data sources, gathering and maintaining the data needed, and completing and reviewing the collection of information. Send comments regarding this burden estimate or any other aspect of this collection of information, including suggestions for reducing this burden, to Washington Headquarters Services, Directorate for Information Operations and Reports, 1215 Jefferson Davis Highway, Suite 1204, Arlington, VA 22202-4302, and to the Office of Management and Budget, Paperwork Reduction Project (0704-0188), Washington, DC 20503.

1. AGENCY USE ONLY (Leave blank)		2. REPORT DATE 30 January 1998	3. REPORT TYPE AND DATES COVERED Final Report for 1 SEPTEMBER 1994 to 30 November 1997	
4. TITLE AND SUBTITLE (U) Turbulence-Chemistry Models In Highly Strained Non-Premixed Flames			5. FUNDING NUMBERS  PE-61102F PR-2308 SA-BS C-F49620-94-C-0020	
6. AUTHOR(S)  Sanjay M. Correa and Iris Z. Hu				
7. PERFORMING ORGANIZATION NAME(S) AND ADDRESS(ES)  General Electric Corporate Research and Development Center P.O. Box 8, K1-ES112 Schenectady, NY 12301			8. PERFORMING ORGANIZATION REPORT NUMBER  AFRL-SR-BL-TR-98-	
9. SPONSORING/MONITORING AGENCY NAME(S) AND ADDRESS(ES)  AFOSR/NA 110 Duncan Avenue, Suite B115 Bolling AFB, DC 20332-0001				
11. SUPPLEMENTARY NOTES				
12a. DISTRIBUTION/AVAILABILITY STATEMENT  Approved for public release; Distribution unlimited				
13. ABSTRACT To allow implementation of chemical kinetic schemes of <i>arbitrary complexity</i> in computational design codes for gas-turbine combustion, a new microstructural turbulent combustion model was developed. The fine structure of turbulent combustion was represented by PSR (Perfectly Stirred Reactor) theory. The theory is the intense-combustion analog of flamelet theory. Residence times in the PSR were related to the scalar dissipation, and turbulence-chemistry interactions were closed by using the probability distribution function for scalar dissipation in a turbulent flow. Calculations compared very favorably with Raman data on temperature and species from three turbulent bluff-body stabilized laboratory flames: (i) a non-premixed CO/H <sub>2</sub> /N <sub>2</sub> -air flame, (ii) a non-premixed CH <sub>4</sub> /H <sub>2</sub> -air flame, and (iii) a premixed CH <sub>4</sub> -air flame. With this success, the model was applied to two practical combustors: (iv) an axially-staged combustion system which produces about half the NO <sub>x</sub> of a conventional combustor while offering greater operability, and operates in an unusual regime of turbulence-chemistry interactions, and (v) a conventional aircraft engine combustor. In the latter case, a kinetic scheme with over 121 species and 996 elementary reactions was demonstrated. In both cases, the calculated results agreed well with temperature and species data. The physical model developed here was used directly in the industry-standard pressure-corrected mean Navier-Stokes/assumed-shape pdf/k-ε type of CFD code, which affords significant geometric flexibility and rapid convergence for gas-turbine combustor flowfields.				
14. SUBJECT TERMS Turbulent combustion modeling; finite-rate chemistry; mixing models		DTIC QUALITY INSPECTED 2		15. NUMBER OF PAGES 64
				16. PRICE CODE
17. SECURITY CLASSIFICATION OF REPORT: UNCLASSIFIED	18. SECURITY CLASSIFICATION OF THIS PAGE: UNCLASSIFIED	19. SECURITY CLASSIFICATION OF ABSTRACT: UNCLASSIFIED	20. LIMITATION OF ABSTRACT UL	

## Section 1

### SUMMARY

This final report describes work performed in the period September 1994 to November 1997 for the U.S. Air Force Office of Scientific Research (AFOSR) under Contract No. F49620-94-C-0020. Dr. Julian Tishkoff was the AFOSR Project Monitor. The work was performed and the report has been prepared by the Mechanical Systems Laboratory at the GE Corporate Research and Development Center, Schenectady, New York. This section summarizes the technical work.

Aeropropulsion gas-turbines generally employ non-premixed turbulent combustion. These engines have aggressive design objectives - including supercruise, increasing thrust:weight ratio, low observables in the exhaust, improved high-altitude performance, endothermic fuel capability, and low pollutant emissions - which in turn lead to new challenges for the combustion system: decreasing size, increasing combustor temperature rise, and low emissions of pollutants, smoke and other visibles. Chemical kinetics and their interactions with turbulence control these phenomena. Although the hypothesis of fast chemistry or "mixed-is-burned" is useful for understanding traditional design issues such as equilibrium exit temperature fields ("pattern factor"), it cannot address these challenges.

The goal of this three-year research program was a quantitative understanding of turbulence-chemistry interactions in the above systems, with a desired outcome of improving CFD-based design tools. This goal has been met, by successfully performing the following tasks.

#### Statement of Work and Synopsis of Results

##### **Task A: Develop and demonstrate a chemistry scheme for fuels more complex than methane.**

Detailed schemes for kerosene-type fuel and for other complex hydrocarbon fuels, such as propane, were identified from literature sources.

##### **Task B: Develop and demonstrate mixing models that are more accurate than the Interaction-by-Exchange-with-the-Mean (IEM) model, while maintaining high parallel efficiency for modern computer architectures.**

A PSR microstructural model was developed for the "distributed reaction" regime. It allows arbitrarily complex multi-step chemistry. The above detailed schemes were incorporated in the PSR microstructural model for greater chemical kinetic accuracy. Up to 1000-step kinetic schemes were demonstrated in 2D PDF-based CFD calculations.

##### **Task C: Compile chemical species and temperature data in the regime of high turbulence intensity.**

Laser-spectroscopic data from three bluff-body stabilized laboratory flames with CO/H<sub>2</sub> and CH<sub>4</sub> fuels were collected. Gas-sampling probe and thermocouple data were compiled from tests of two practical combustors. All these flames were in the highly-strained regime where non-equilibrium effects are pre-dominant.

##### **Task D: Extend the PDF/mean-flow-computational fluid dynamic (CFD) model to the above high turbulence experiments and compare the results of the calculations with the data.**

The PSR microstructural model (see Task B) was applied to the three bluff-body stabilized flames and the two practical combustors (see Task C).

## Section 2

### TECHNICAL DISCUSSION

Despite significant progress, it is not clear how turbulent combustion should be viewed. Conceptual questions arise such as whether turbulent flames act as ensembles of strained laminar "flamelets" or as broader "distributed" zones of reacting species. Engineering models of combustors rely largely on simple approaches such as fast chemistry (mixed is burned) and assumed shape probability density functions (pdf's), and have been successful in terms of gross features such as the profiles of combustor exit temperature. Present-day demands on combustion equipment and thus on computational models are, however, increasing the need for advanced understanding of turbulence-chemistry interactions. For example, (i) flameout and relight in turbine combustors are related to interactions with chain-branching reactions, (ii) hydrogen burnout in supersonic combustors is related to interactions with recombination reactions, and (iii) requirements of low emissions of  $\text{NO}_x$ , CO, smoke, and other observables are related to non-equilibria among species such as oxyhydrogen radicals and  $\text{C}_x\text{H}_y$ . These turbulence-chemistry interactions span several orders of magnitude in Damkohler number (ratio of turbulent mixing to chemical time-scale), depending on the specific reaction and the specific turbulence process in question.

This lack of a theoretical framework prevents industry from having reliable combustor design tools.

Computational modeling needs to be improved because of the high cost of prototype development and testing. Today, products are often planned and sales efforts are launched on the basis of predicted performance, and metal is not actually cut until customers are lined up. Models must therefore address all the issues of concern to customers, as outlined above. This is a more ambitious set of parameters than the traditional requirement of only the pattern factor.

This research program addressed the technical issues by the development (and detailed validation) of computational models that fit into a familiar framework. Otherwise the design and development communities would not be able to use the results. It also seems clear that different modeling approaches will be needed to address different issues. Unsteady methods such as Large Eddy Simulation or Discrete Vortex Models may be used to isolate features of the flowfield, such as mixing layers. Direct Numerical Simulation will play a role in physical sub-model development. These methods, however, will not directly transfer information to the majority of engineers. The present pdf methods are superior to others in the context of gas-turbine combustion.

A new sub-model for the simulation of the interaction between turbulence and full chemistry schemes has been developed. We argue that it is superior to other tools such as the strained laminar flame. It traces a direct lineage from pdf/CFD models as shown below. Also, it is important to note that the new model fits into the industry-standard CFD approach: pressure-corrected mean Navier-Stokes/assumed-shape pdf/ $k-\epsilon$  turbulence model which affords significant geometric flexibility and rapid convergence for gas-turbine combustor and similar pressure-dominated internal flows [Correa and Shyy (1987)].

The following sub-sections highlight the approach and the results.

## 2.1 Transition of Monte Carlo PDF Techniques to Practical Combustor Design Codes

Applications of the particle-tracking reduced-chemistry PDF model were supported using GE's 3D combustor design code "CONCERT" (Cartesian Or Natural Coordinates for Elliptic Reacting Turbulent flows). CONCERT is used to design all GE's aeropropulsion turbine engines, both military and commercial, and including main combustion chambers and augmentors. Previously, CONCERT used the standard assumed-shape pdf approach in which the shape of the pdf for the mixture fraction (and a reaction progress variable if desired) was assumed in terms of its lowest moments, which were solved for from transport equations within CONCERT.

In the Monte Carlo PDF version, CONCERT used particle tracking for the scalar(s) pdf (Tolpadi et al., 1996). Figure 1 depicts the information flow between the modules of the code.

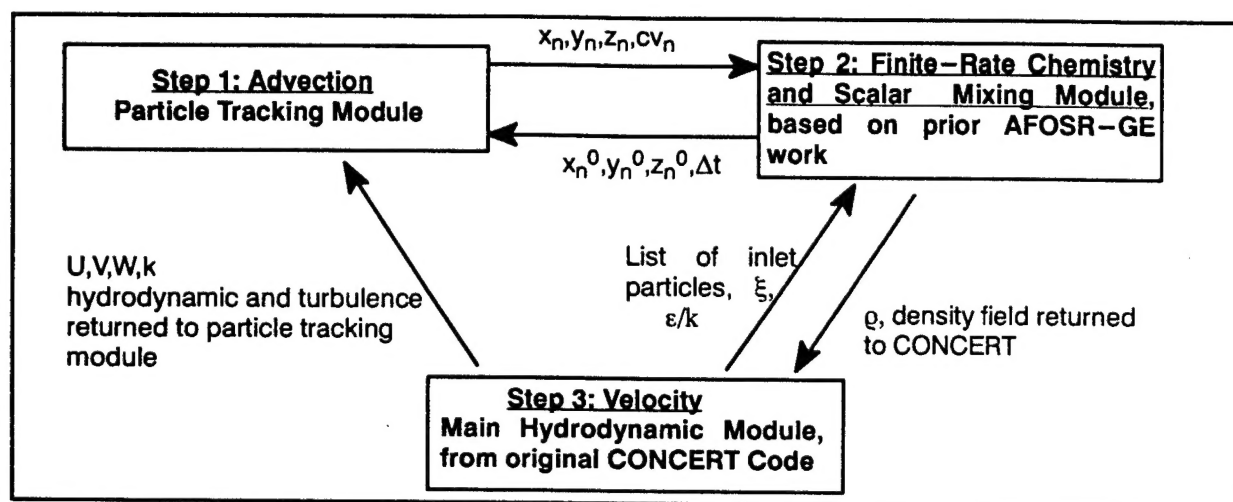


Figure 1. Information flow between modules of the CONCERT Monte Carlo PDF Model.

The design code implementation and calculations were carried out under GE (not AFOSR) funding. CONCERT continues to be the primary vehicle for transition of research from this contract.

## 2.2 Chemical Kinetics of Complex Hydrocarbons

Kinetic schemes for complex hydrocarbon fuels – approaching aviation jet fuel – were identified from literature sources [Gueret et al. (1990); Dagaut et al. (1994); Dagaut et al. (1996)], along with additional work in progress.

A full chemical mechanism for propane combustion was assembled by Konnov [1997]. The mechanism contains an oxidation reaction set for hydrocarbons C1–C3 and their derivatives, N–H–O chemistry and in-flame NOx formation. The basic C/H/O C1–C2 reaction mechanism originated from the methane combustion mechanism [Borisov et al. (1982)] and was extended to cover reactions for methanol, acetaldehyde, ethanol and ethylene oxide. It was largely revised using several sources [Tan et al. (1994), Ranzi et al. (1994); Warnatz (1984)] and updated on the basis of recommendations of the European Evaluation

Group [Baulch et al. (1994)]. The C/H/N/O reaction sub-mechanism was developed on the basis of the widely used Miller–Bowman [1989] scheme with many additional reactions from other sources. The entire mechanism consists of 996 reactions among 121 species. The mechanism was assembled in the CHEMKIN format. Thermodynamic data associated with this scheme were taken from Burcat and McBride [1997].

### 2.3 Turbulent Combustion Model Based on PSR Microstructure and Full Kinetic Schemes

Given the complexity of the phenomena and fuels of interest, full rather than reduced chemistry schemes will probably be required. In principle, the laminar flamelet model (LFM) is available [Peters (1986)]. In the context of intensely turbulent combustion, however, the LFM breaks down because the reaction zone is not thin and the fluctuation of mixture fraction in the reaction zone is not small [Bilger (1988)]. Hence an alternative to the LFM was developed.

#### 2.3.1 Non-Premixed Flames

In a non-premixed turbulent flame, the thermochemical properties can be characterized by the mixture fraction and the reaction residence time. From the Lagrangian point of view, the residence time is the time for a reactive "particle" to travel through the flow field. This time depends on the mean flow as well as on turbulent fluctuations. In intensely turbulent flames, the latter is more significant to the residence time than the former. Turbulent scalar fluctuations are diminished in magnitude by scalar dissipation. Therefore, the residence time may be quantified using scalar dissipation rate. The lower the dissipation rate, the more time there is for reactions (i.e., the larger microscale residence time). Furthermore, turbulent flame properties can be described by the pdf's of mixture fraction and scalar dissipation rate (or microscale residence time).

As a first step in the modeling, fluctuations in the mixture fraction  $\xi$  and the scalar dissipation rate  $\chi$  are assumed to be statistically independent. Therefore, their joint pdf  $P(\chi, \xi)$  is separable

$$P(\chi, \xi) = P_1(\chi) P_2(\xi) \quad (1)$$

Following Liew et al. [1984], the pdf of the scalar dissipation rate  $\chi$  is taken to be log-normal

$$P_1(\chi) = \frac{1}{\chi \sigma \sqrt{2\pi}} \exp \left[ -\frac{(\ln \chi - \mu)^2}{2\sigma^2} \right] \quad (2a)$$

where  $\mu$  is the mean and  $\sigma$  is the standard deviation of  $\ln \chi$ . These two parameters are related to the mean scalar dissipation rate  $\bar{\chi}$  and local turbulent Reynolds number  $Re$  as

$$\bar{\chi} = \exp \left[ \mu + \frac{\sigma^2}{2} \right] \quad (2b)$$

and

$$\sigma^2 = \frac{1}{2} \ln \frac{\sqrt{Re}}{10} \quad (2c)$$

The mean scalar dissipation rate  $\bar{\chi}$  is related to the local turbulence kinetic energy  $k$ , the local dissipation rate  $\epsilon$ , and the local variance of mixture fraction  $\bar{g}$ , as follows

$$\bar{\chi} = C_{\varphi} \frac{\varepsilon}{k} \bar{g} \quad (3)$$

where  $C_{\varphi 2}$  is a constant in the  $k-\varepsilon-g$  model [Liew et al. (1984)].

Magnussen et al. [1979] related the residence time " $\tau$ " in the fine scales to the turbulence dissipation rate  $\varepsilon$

$$\tau = (\nu/\varepsilon)^{1/2} \quad (4)$$

where  $\nu$  is the laminar viscosity. Eq. (4) ascribes a single residence time to the scales of chemical reactions. As stated above, the residence time depends on turbulent fluctuations and hence, on (the pdf of) scalar dissipation. A relationship between instantaneous residence time and instantaneous scalar dissipation rate in the large scales is proposed here

$$\tau = C \frac{\bar{g}}{\bar{\chi}} \quad (5)$$

where  $C$  is a constant. After calculations of different non-premixed flames – as reported in the following sections – the constant  $C$  in Eq. (5) was taken to be 10. Based on Eq. (5),  $P(\tau)$  can be obtained from  $P(\chi)$  as

$$P(\tau) = \frac{\chi^2}{C \bar{g}} P_1(\chi) \quad (6)$$

$P_2(\xi)$  is assumed to be a beta function [Correa and Shyy (1987)],

$$P_2(\xi) = \frac{\xi^{a-1} (1-\xi)^{b-1}}{\int_0^1 \xi^{a-1} (1-\xi)^{b-1} d\xi} \quad (7a)$$

where the parameters " $a$ " and " $b$ " are related to the local mean and variance of the fluctuations in the mixture fraction,

$$a \equiv \bar{\xi} \left( \frac{\bar{\xi}(1-\bar{\xi})}{\bar{g}} - 1 \right), \quad b \equiv (1-\bar{\xi}) \left( \frac{\bar{\xi}(1-\bar{\xi})}{\bar{g}} - 1 \right) \quad (7b)$$

Hence, the joint pdf of the mixture fraction and the residence time is obtained as

$$P(\xi, \tau) = \frac{\chi^2}{C \bar{g}} P_1(\chi) \frac{\xi^{a-1} (1-\xi)^{b-1}}{\int_0^1 \xi^{a-1} (1-\xi)^{b-1} d\xi} \quad (8)$$

Finally, the mean of a thermochemical quantity  $\bar{\phi}_k$  (where " $k$ " represents the species mass fractions, density, and temperature) at a point in the turbulent reacting gas is obtained by convolution with the pdf at that point

$$\bar{\phi}_k = \int_0^{\infty} \int_0^1 \phi_k(\xi, \tau) P(\xi, \tau) d\xi d\tau \quad (9)$$

where  $\phi_k(\xi, \tau)$  describes the dependence of  $\phi_k$  on mixture fraction and residence time.

The dependence of  $\phi_k$  on mixture fraction and residence time is computed by exercising a PSR code over the allowable range of mixture fractions  $\xi$  and residence times  $\tau$ , using a full chemical kinetic scheme.

At each point in the  $\xi$ - $\tau$  space, the computed species mass fractions, densities, and temperatures are tabulated in a two-dimensional library for use during the "hydrodynamic" calculation.

Hence, in this approach, the hydrodynamic field equations to be computed are continuity, the components of the mean momentum equation,  $k$ ,  $\epsilon$ , and the mean and variance of the mixture fraction. The mean density of reacting gas is updated iteratively when solving these equations.

### 2.3.2 Comparison with Non-Premixed CO/H<sub>2</sub>/N<sub>2</sub>-Air Flame

The first case is a non-premixed bluff-body stabilized CO/H<sub>2</sub>/N<sub>2</sub>-air flame. The kinetic scheme of Table 1 was used in the model. The non-premixed reactants are a fuel mixture comprised of 27.5%CO/32.3%H<sub>2</sub>/40.2%N<sub>2</sub> and air, at a pressure of one atmosphere and an inlet temperature of 300K [Correa and Gulati (1992)]. The cylindrical axisymmetric bluff body has an outer diameter of 38.1 mm with an axial jet of diameter "d" of 3.18 mm located in the center (Fig. 2). It is well known that parts of such flow fields – notably, the annular shear layer shed off the bluff body – can be dominated by unsteady effects. Care was taken to operate in a velocity (jet and coflow) regime where the flame was steady. The cold jet Reynolds number was 12,000, based on the jet diameter and jet exit velocity of 80 m/s. The coflow air velocity is 6.5 m/s. The back surface of the bluff body was coated with a thermal barrier material to reduce heat loss. The flame was stabilized by the recirculation zone provided by the bluff body. The tunnel cross-section was 15 cm. x 15 cm., large enough not to interfere with the flame. (The calculations discussed below were made for a circular duct of the same cross-sectional area).

Table 1. Kinetic Mechanism Used for CO/H<sub>2</sub>-Air Combustion.

(Forward rate constant  $k_f = A T^b e^{-E/RT}$ , moles-cm-s-K; E units: cal/mole)

No.	Reaction	A	b	E
1.	CO+O+M=CO <sub>2</sub> +M	3.20E+13	0.0	-4200.0
2.	CO+OH=CO <sub>2</sub> +H	1.51E+07	1.3	-758.0
3.	CO+O <sub>2</sub> =CO <sub>2</sub> +O	1.60E+13	0.0	41000.0
4.	HO <sub>2</sub> +CO=CO <sub>2</sub> +OH	5.80E+13	0.0	22934.0
5.	H <sub>2</sub> +O <sub>2</sub> =2OH	1.70E+13	0.0	47780.0
6.	OH+H <sub>2</sub> =H <sub>2</sub> O+H	1.17E+09	1.3	3626.0
7.	H+O <sub>2</sub> =OH+O	2.00E+14	0.0	16800.0
8.	O+H <sub>2</sub> =OH+H	1.80E+10	1.0	8826.0
9.	H+O <sub>2</sub> +M=HO <sub>2</sub> +M	2.10E+18	-1.0	0.0
H <sub>2</sub> O enhanced by 21.0, CO <sub>2</sub> enhanced by 5.0, H <sub>2</sub> enhanced by 3.3, CO enhanced by 2.0, O <sub>2</sub> enhanced by 0.0, N <sub>2</sub> enhanced by 0.0				
10.	H+O <sub>2</sub> +O <sub>2</sub> =HO <sub>2</sub> +O <sub>2</sub>	6.70E+19	-1.4	0.0
11.	H+O <sub>2</sub> +N <sub>2</sub> =HO <sub>2</sub> +N <sub>2</sub>	6.70E+19	-1.4	0.0
12.	OH+HO <sub>2</sub> =H <sub>2</sub> O+O <sub>2</sub>	5.00E+13	0.0	1000.0
13.	H+HO <sub>2</sub> =2OH	2.50E+14	0.0	1900.0
14.	O+HO <sub>2</sub> =O <sub>2</sub> +OH	4.80E+13	0.0	1000.0
15.	2OH=O+H <sub>2</sub> O	6.00E+08	1.3	0.0
16.	H <sub>2</sub> +M=H+H+M	2.23E+12	0.5	92600.0
H <sub>2</sub> O Enhanced by 6.0, H enhanced by 2.0, H <sub>2</sub> enhanced by 3.0				
17.	O <sub>2</sub> +M=O+O+M	1.85E+11	0.5	95560.0
18.	H+OH+M=H <sub>2</sub> O+M	7.50E+23	-2.6	0.0
H <sub>2</sub> O enhanced by 21.0				
19.	H+HO <sub>2</sub> =H <sub>2</sub> +O <sub>2</sub>	2.50E+13	0.0	700.0
20.	HO <sub>2</sub> +HO <sub>2</sub> =H <sub>2</sub> O <sub>2</sub> +O <sub>2</sub>	2.00E+12	0.0	0.0
21.	H <sub>2</sub> O <sub>2</sub> +M=OH+OH+M	1.30E+17	0.0	45500.0
22.	H <sub>2</sub> O <sub>2</sub> +H=HO <sub>2</sub> +H <sub>2</sub>	1.60E+12	0.0	3800.0
23.	H <sub>2</sub> O <sub>2</sub> +OH=H <sub>2</sub> O+HO <sub>2</sub>	1.00E+13	0.0	1800.0

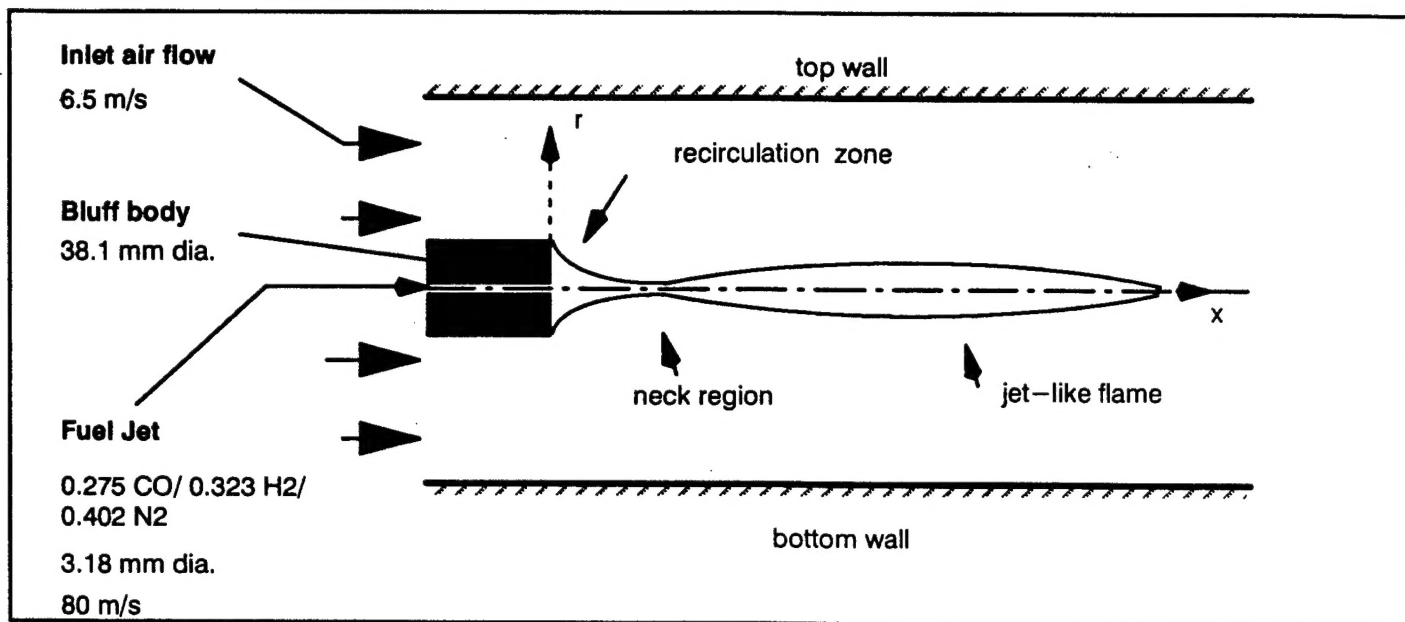


Figure 2. The non-premixed CO/H<sub>2</sub>/N<sub>2</sub>-air flame.

Calculated quantities are compared with Raman data at two axial locations ( $x/d=10$ ,  $x/d=20$ , where  $d$  is the jet diameter), which are in this highly strained part of the flame. Calculated radial profiles of the mean temperature (Fig. 3, where  $r$  is the radial distance from the center line), the mean mass fraction of CO (Fig. 4), and the mean mass fraction of H<sub>2</sub>O (Fig. 5) compare very well with the data, at both locations.

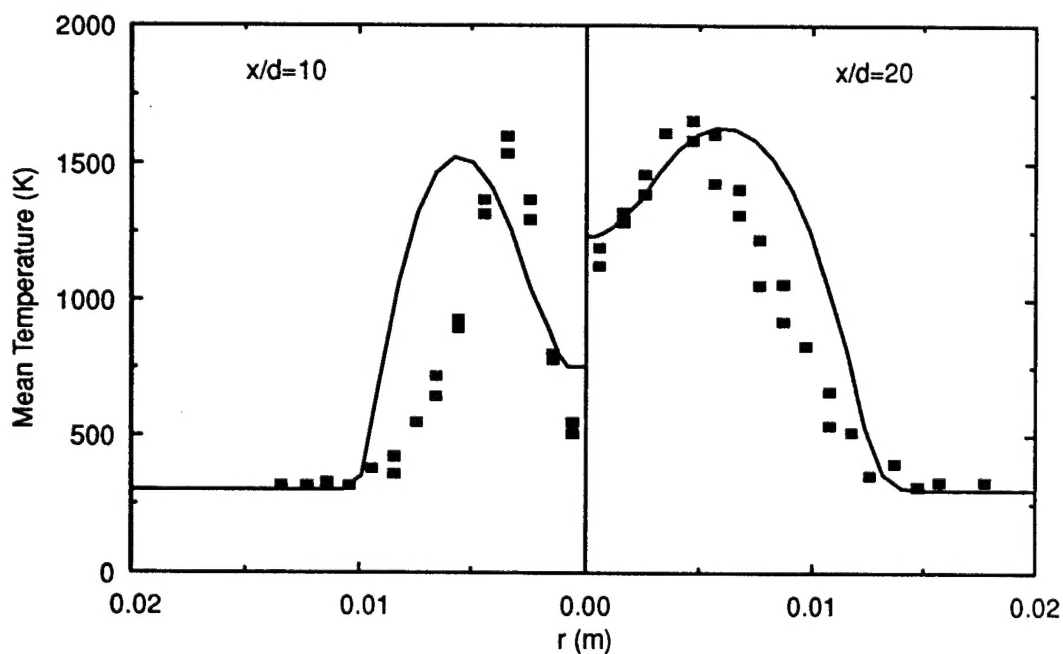


Figure 3. Comparison of calculated temperature profiles with Raman data in CO/H<sub>2</sub>/N<sub>2</sub>-air flame.

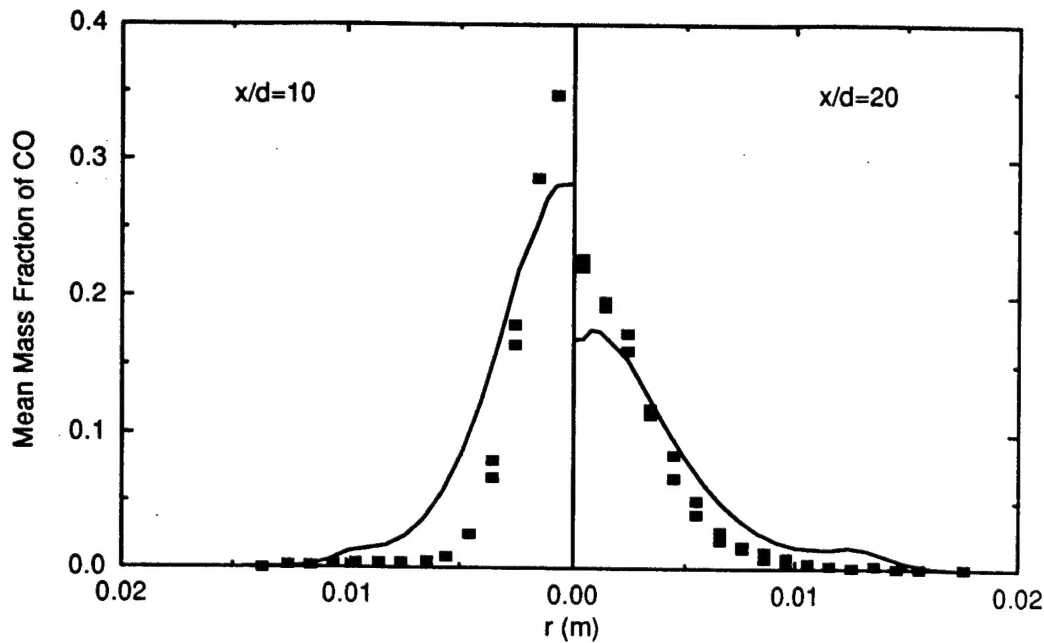


Figure 4. Comparison of calculated CO profiles with Raman data in CO/H<sub>2</sub>/N<sub>2</sub>–air flame.

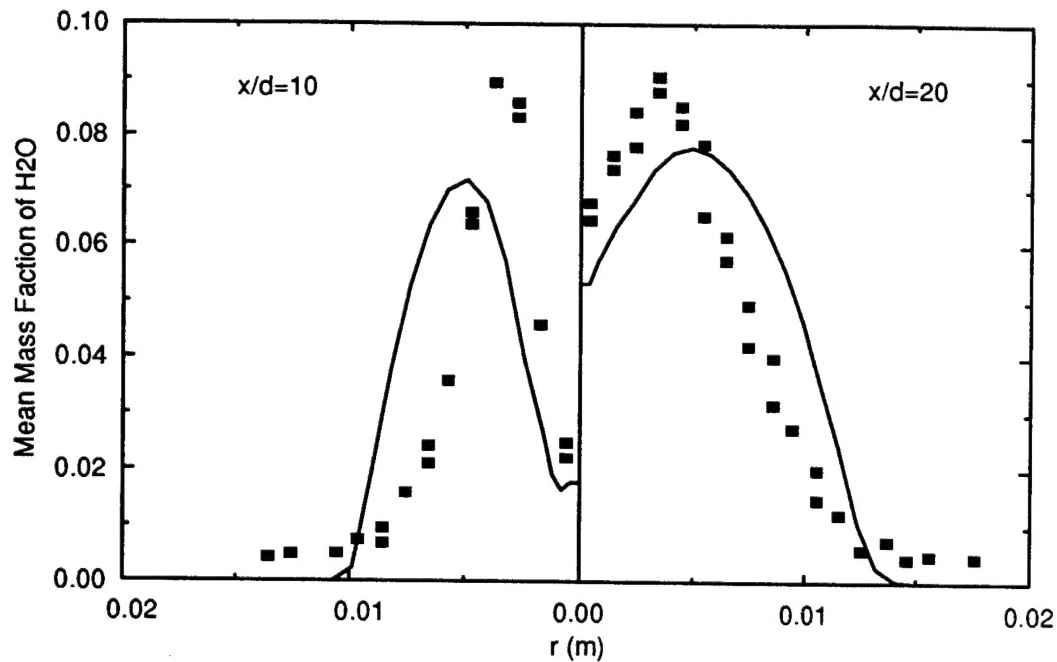


Figure 5. Comparison of calculated H<sub>2</sub>O profiles with Raman data in CO/H<sub>2</sub>/N<sub>2</sub>–air flame.

Data and calculations both show the annular shear–layer nature of the flame and the (kinetically–limited) cool fuel–rich nature of the jet core at  $x/d=10$ . The profiles become more uniform by  $x/d=20$ , as the centerline region starts to burn. Hence, the PSR–microstructure model is adequate for calculation of the mean features (at least) of this non–premixed CO/H<sub>2</sub>/N<sub>2</sub>–air flame.

### 2.3.3 Comparison with Non-Premixed $\text{CH}_4/\text{H}_2$ -Air Flame

Non-premixed methane flames are of interest because CO emissions, particularly at part-load combustor operation, are of great concern to combustion system designers. CO emissions are difficult to calculate because of the interplay between CO production by pyrolysis of fuel, CO consumption (primarily by  $\text{CO} + \text{OH} = \text{CO}_2 + \text{H}$  beyond the pyrolysis region of a flame), and the quenching imposed by the turbulent flow field. The data used for comparison are from the experiment of Masri et al. [1992]. The burner has a bluff body diameter of 50 mm, a central fuel jet diameter of 2 mm, fuel composition  $\text{CH}_4/\text{H}_2 = 2:1$  by volume, and fuel jet velocity 167.1 m/s (Fig. 6). Co-flowing air at 25 m/s is supplied through an 86 mm (inner diameter) shroud, which is itself surrounded by tunnel co-flow at 2 m/s. The  $\text{H}_2$  contained in the fuel prevents soot formation in the flame.

The kinetic mechanism, of Table 2 was used in the calculation.

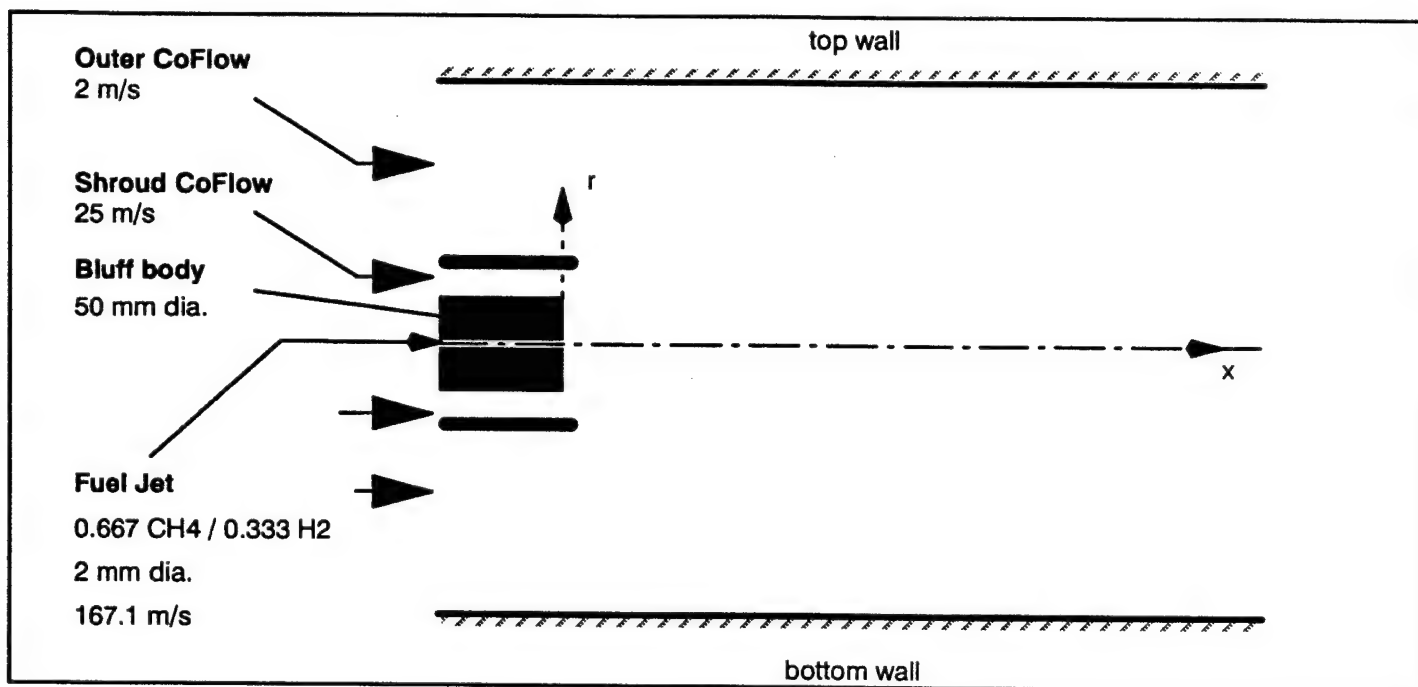


Figure 6. The non-premixed  $\text{CH}_4/\text{H}_2$ -air flame.

When the hydrodynamic field equations with the standard  $k-\epsilon$  model were computed for this flow-field, it was found that the measured mean mixture fraction profiles were not matched closely enough to properly assess the concept of PSR-based microstructure. Qualitatively speaking, the calculated results using the  $k-\epsilon$  model matched what was found in the experiments. For example, two vortices were observed behind the bluff body, which indicates a complex flow structure formed at a critical balance between the annular and jet flow momenta. The center of the outer vortex is at about the same location as in the experiments, while the location of the inner vortex deviates from what was described by Masri et al. [1992]. The inaccurate calculation of the inner vortex is the main reason for the discrepancies in the mixture fraction field. Various modifications of the  $k-\epsilon$  model were tried but without success. Correspondence with the authors [Masri (1995)] revealed that other groups have had difficulty in computing this flowfield. To permit progress in assessment of the micro-structure model, the measured mean and variance fields of the mixture fraction [Masri et al. (1992)] were used in lieu of the fields from the CFD calculation.

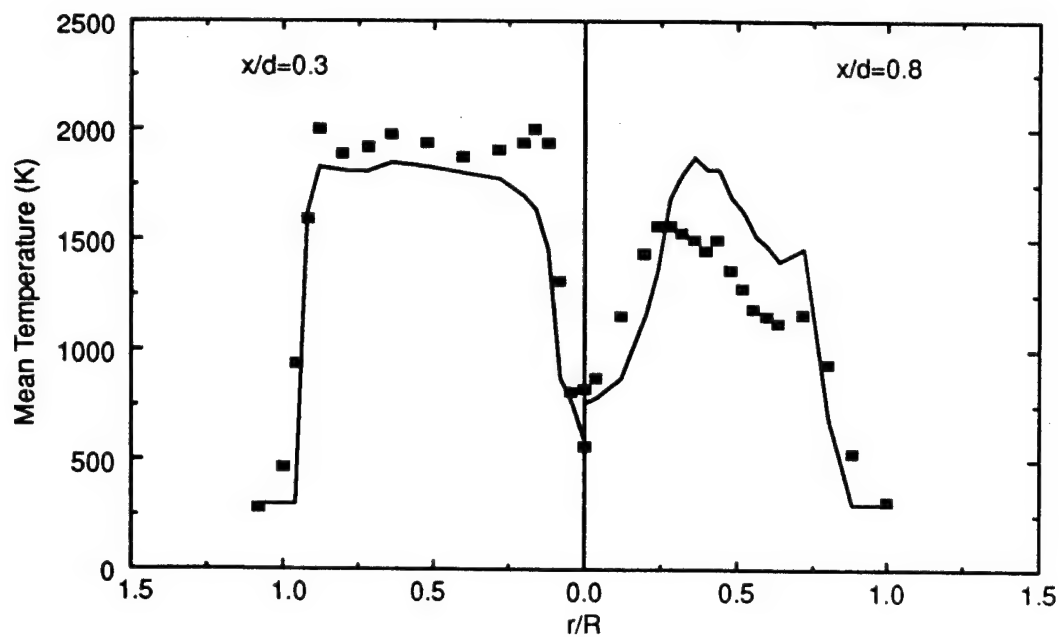


Figure 7. Comparison of calculated temperature profiles with Raman data in  $\text{CH}_4/\text{H}_2$ -air flame.

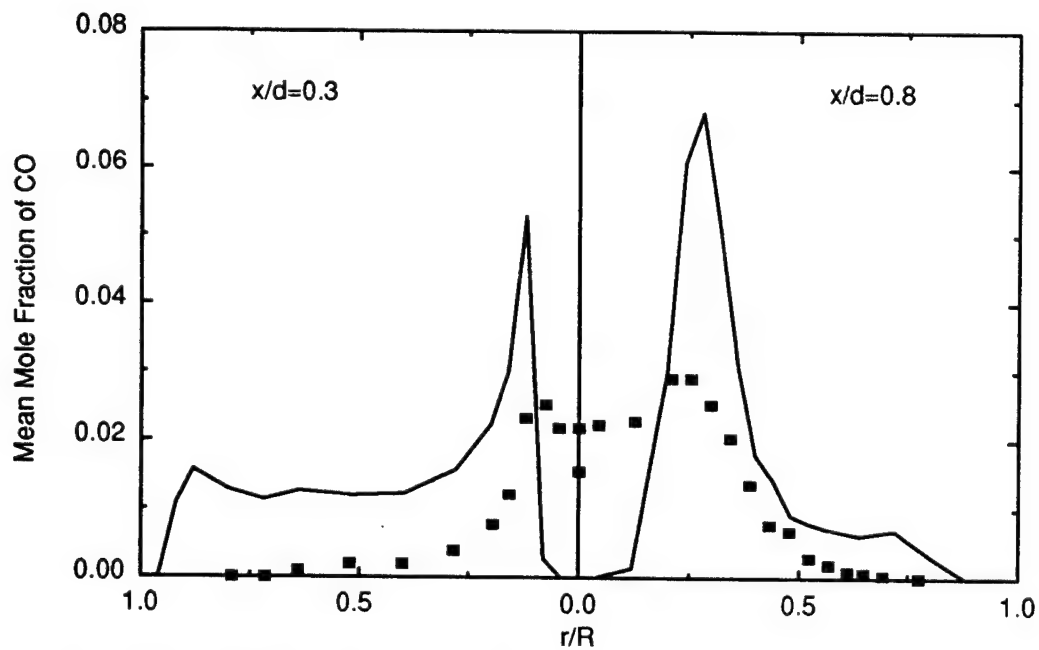


Figure 8. Comparison of calculated CO profiles with Raman data in  $\text{CH}_4/\text{H}_2$ -air flame.

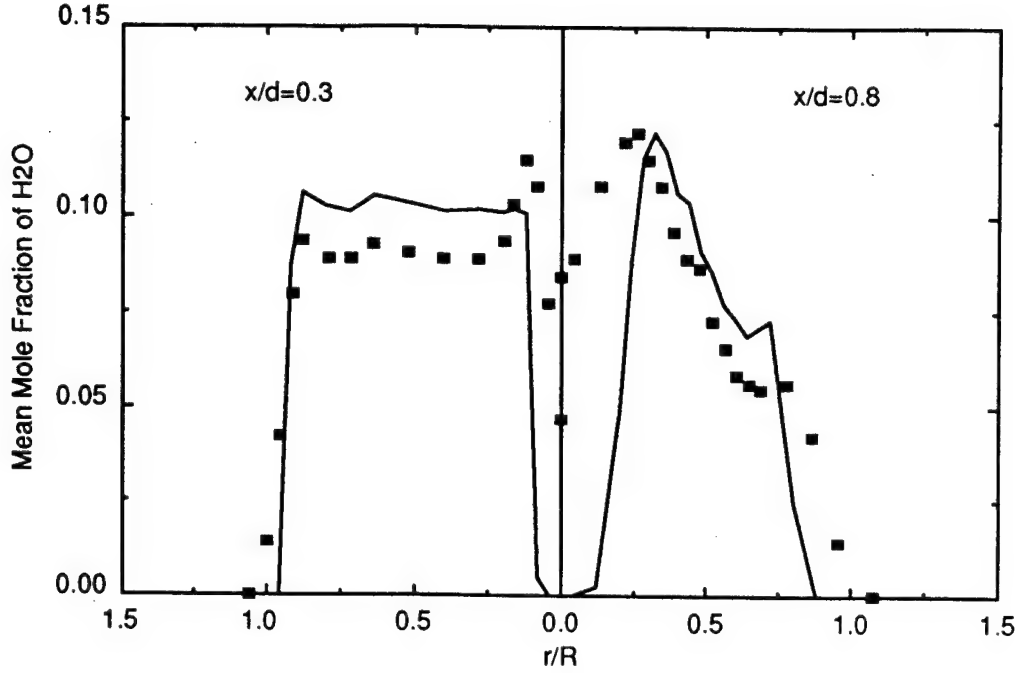


Figure 9. Comparison of calculated H<sub>2</sub>O profiles with Raman data in CH<sub>4</sub>/H<sub>2</sub>-air flame.

Hence, even though the hydrodynamic field could not be calculated accurately enough with the  $k-\epsilon$  model, it could be shown that the PSR-microstructure model reproduced the following important features of this non-premixed CH<sub>4</sub>/H<sub>2</sub>-air flame: (i) in the high shear region, because of the high scalar dissipation rate, the residence time is small. Therefore, there are significant non-equilibrium effects (shown by low temperature and high CO level); (ii) in the outer vortex region, the gas is close to equilibrium.

### 2.3.4 Premixed Flames

In the case of premixed flames, there is no need to carry the mixture fraction as a variable and the thermochemical properties become a function of residence time alone. The mean thermochemical quantity at a point becomes

$$\bar{\Phi}_k = \int_0^{\infty} \Phi_k(\tau) P(\tau) d\tau \quad (10)$$

and the pdf  $P(\tau)$  is needed throughout the flow field.

Since the mixture fraction is uniform in a premixed flame, calculation of  $P(\tau)$  cannot depend on the scalar variance  $\bar{g}$  as in the non-premixed case. Instead, an analogous approach is developed in which the local  $k$  and  $\epsilon$  are used to form the residence time  $\tau = C k / \epsilon$ , where  $C$  is a coefficient, and  $\epsilon$  is the instantaneous turbulence dissipation rate instead of the mean quantity. Similarly to Eq. (6), the pdf of  $\tau$  can be obtained from the pdf of  $\epsilon$  by assuming a log-normal distribution for the latter [Liew et al. (1984)].

The coefficient  $C$  must reflect the fact that at low turbulence intensities "I" there is little mixing and hence little chemical reaction. As a first step, the following simple step function is used in the current model:

$$C=0 \quad \text{for } I < 0.1 \quad (11a)$$

$$C=0.075 \quad \text{for } 0.1 \leq I \leq 0.25 \quad (11b)$$

$$C=3.5 \quad \text{for } I > 0.25 \quad (11c)$$

Hence, in this approach, the calculation of a turbulent premixed flame involves solving the continuity equation, the momentum equations, the two equations for  $k$  and  $\epsilon$  and a one-dimensional convolution of  $P(\tau)$  over a range of  $\tau$  to obtain the mean thermochemical properties.

### 2.3.5 Comparison with Premixed CH<sub>4</sub>–Air Flame

Nandula et al. [1996] describe the experiment (Fig. 10). Premixed CH<sub>4</sub> and air at an equivalence ratio of 0.586 (corresponding to an equilibrium flame temperature of 1641K) flow over an axisymmetric conical flame holder oriented with its vertex pointing upwind. The base diameter of the cone is 44.45 mm, the tunnel is 80 cm. x 80 cm., and the average premixture velocity upstream of the flame–holder is 14.46 m/s.

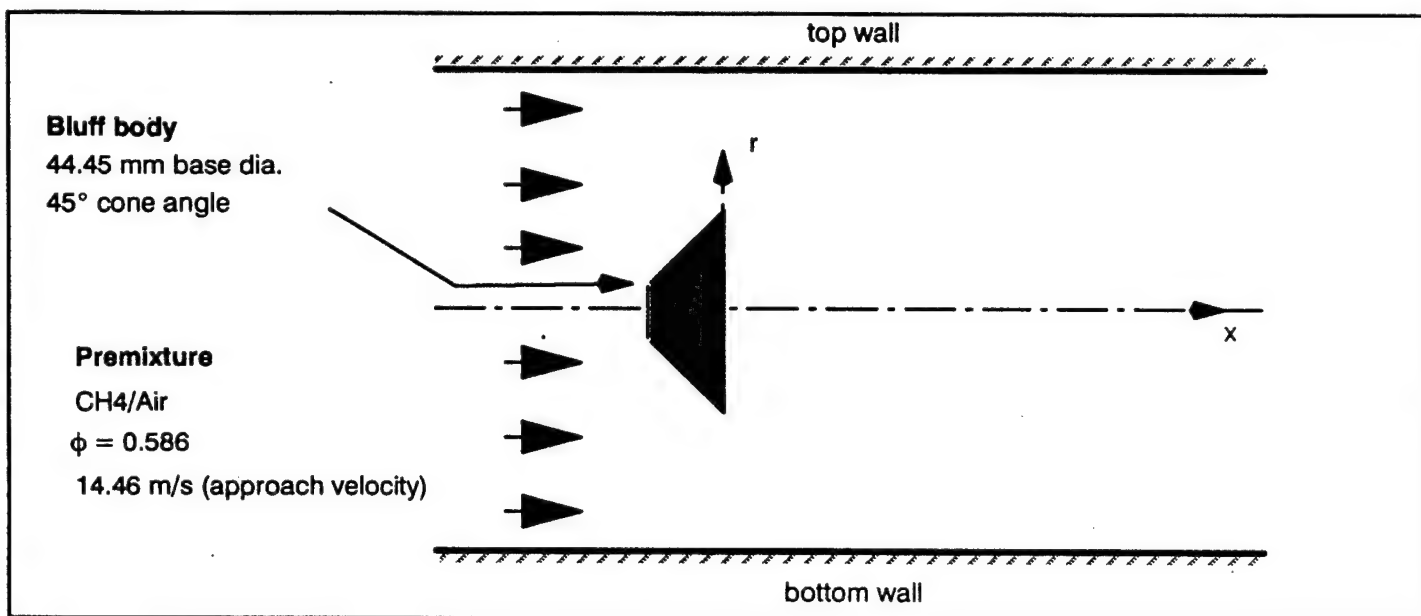


Figure 10. The premixed CH<sub>4</sub>–air flame.

Calculations are compared with Raman data at two axial locations  $x/D=0.1$  and  $x/D=0.6$ , where  $D$  is the base diameter of the cone. The calculated mean temperature profiles agree extremely well with the Raman data at both locations (Fig. 11), although the fairly featureless uniformity of the mean temperature is not a difficult test of the model. The excellent agreement on mean CO at  $x/D=0.1$  (Fig. 12) in terms of both the magnitude and shape of the profile is a much more severe test, because of the competing production–destruction paths involved in the determination of CO as discussed above. The model captures the pronounced non–equilibrium effects in the high shear region. The agreement on CO at  $x/D=0.6$  is as good in the outer (shear layer) part of the flame, but the model significantly overpredicts the CO along the centerline: the model calculates a greater departure from equilibrium than is apparent from the data. Lastly, comparisons of the calculated mean NO with Raman data at both  $x/D=0.1$  and  $x/D=0.6$  (Fig. 13) indicate agreement to within a factor of two.

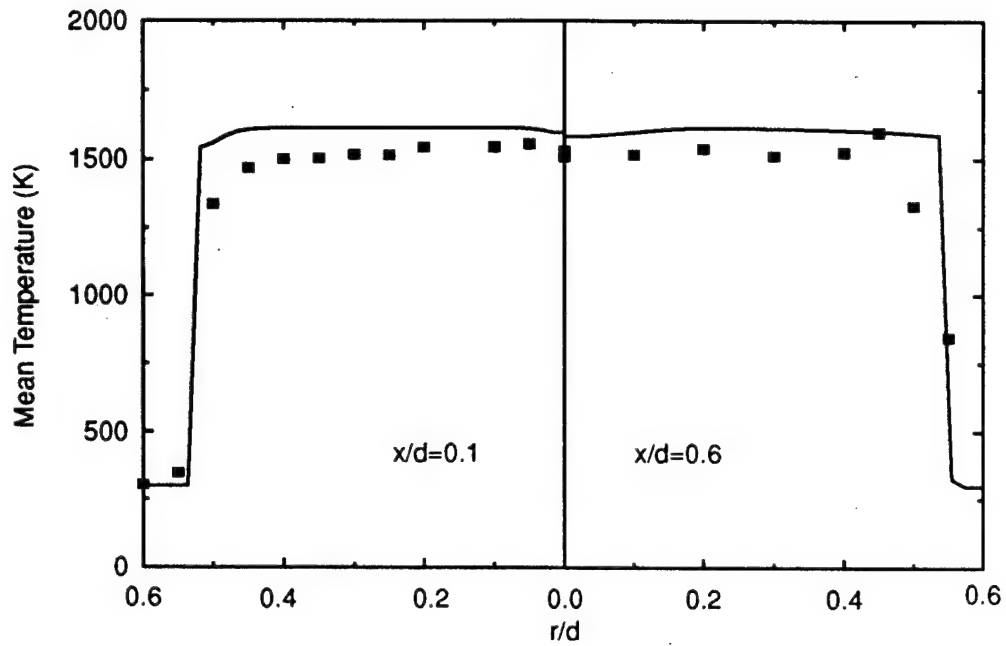


Figure 11. Comparison of calculated temperature with Raman data in the premixed  $\text{CH}_4$ -air flame.

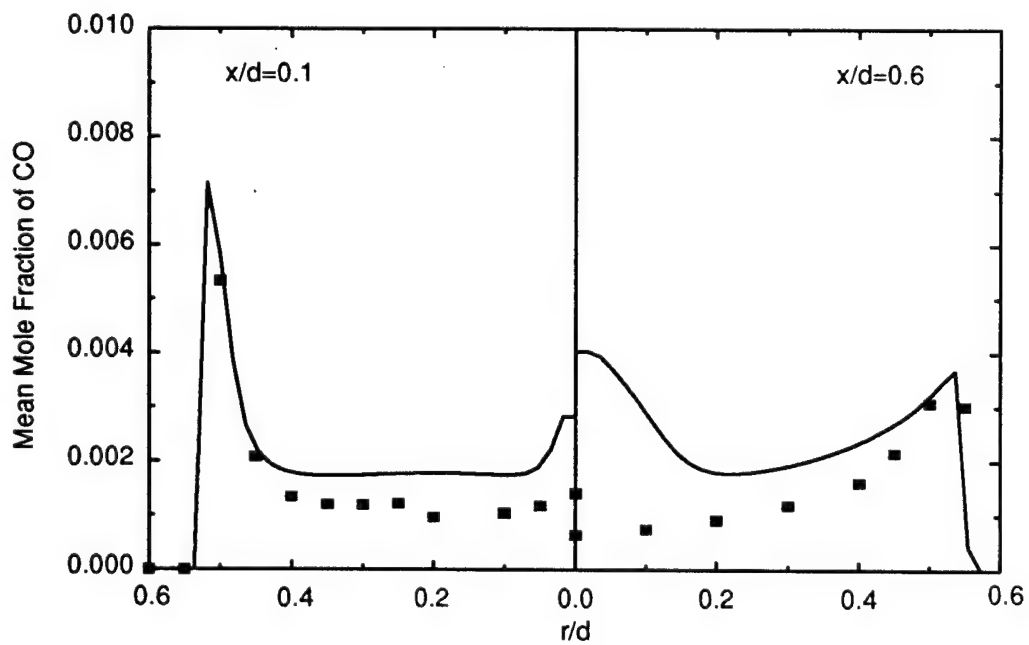


Figure 12. Comparison of calculated CO with Raman data in the premixed  $\text{CH}_4$ -air flame.

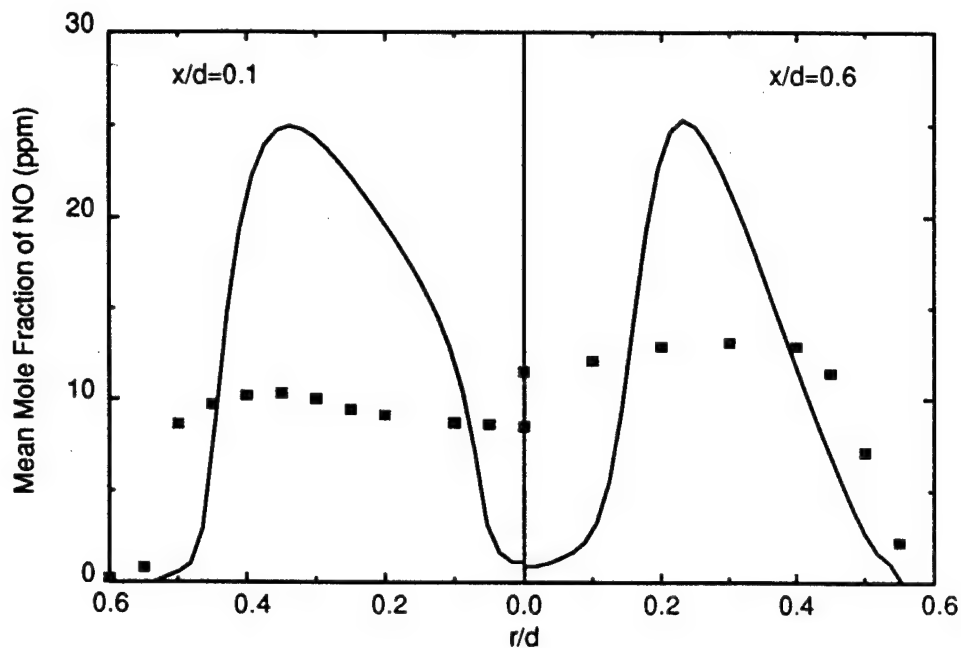


Figure 13. Comparison of calculated NO with Raman data in the premixed CH<sub>4</sub>–air flame.

### 2.3.6 Conclusions from comparison with time- and space-resolved data

The “PSR microstructure model” is developed for turbulent flames in the “distributed reaction zone” regime, and offers an alternative to the laminar flamelet model while retaining the capability of handling full chemical kinetic schemes. The model is implemented in a very straightforward manner in a two-dimensional axisymmetric “k-ε-g” CFD code. Calculations compared favorably with Raman data from three turbulent bluff-body stabilized flames: (i) a non-premixed CO/H<sub>2</sub>/N<sub>2</sub>–air flame, (ii) a non-premixed CH<sub>4</sub>/H<sub>2</sub>–air flame, and (iii) a premixed CH<sub>4</sub>–air flame. The results show that the PSR microstructure model offers an acceptable degree of fidelity despite its simplicity. Calculated profiles are similar to those measured, and the quantitative agreement is generally within 200K or better on mean temperature and within a factor of two or better even on highly non-equilibrium quantities such as CO in a CH<sub>4</sub>–air flame. The computational speed offered by the model – and its compatibility with standard CFD algorithms – makes it an attractive option in practical three-dimensional combustor design calculations, at least as a prelude to more expensive calculations. The level of agreement was excellent given the simplicity and computational speed of the model. Hence, the model was extended to the calculation of practical flames.

## 2.4 Comparison of Calculations with Data from High-Pressure Staged-Combustor

Combustion in vitiated air is of interest in military engine afterburners, in reheat gas-turbines used for power generation, and as axial staging technology for the suppression of emissions without loss of engine operability. It also provides a new regime of turbulence-chemistry interactions: specifically, the ignition of fuel injected in the second burner occurs via reaction pathways which can be quite different from those in conventional systems, given the high temperatures and low oxygen exiting the first burner.

### 2.4.1 Experimental Set-Up

A high-pressure fuel-staged combustion test rig was built at the GE R&D Center (on non-AFOSR funding). Several combustion tests were conducted with different fuel splits between the first and the second burners. The combustor was simulated using the PSR microstructural model, and the calculation demonstrated similar results. In the following sections, the combustion rig, the thermoproperties of methane/vitiated air combustion and the CFD model are described. Results of modeling are analyzed in detail and are also compared with the test results.

Figure 14 shows the configuration of the second burner in the fuel staging rig. The second burner consists of a contraction section, where the fuel is injected, and a combustion chamber. The combustion chamber is a straight pipe 10.16 cm. in diameter, while the contraction section is 5.08 cm. in diameter. The contraction section is about 15.24 cm. long, and the fuel injector is located about half-way down the contraction. The fuel is introduced from a small hole at the tip of a thin tube which extends to the center line of the burner.

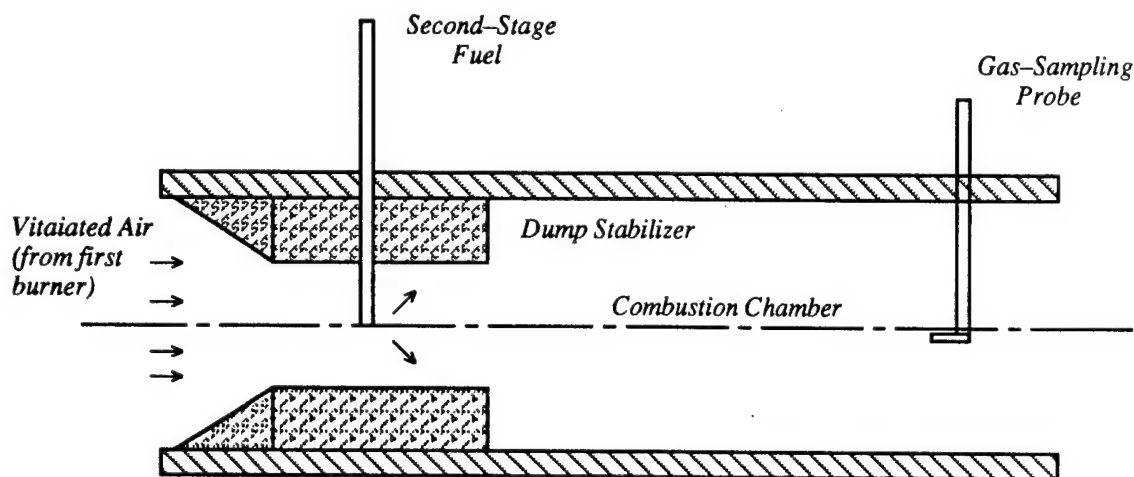


Figure 14. Second-stage burner in staged combustion rig.

### 2.4.2 Thermoproperties and CFD model

In the PSR model, the thermoproperties of burning gas are characterized by two parameters: mixture fraction and residence time. In the case of the second stage burner, the mixture fraction is defined as the mass fraction of Feed 2 (fuel) in the total mixture (Feed 1 + Feed 2). Therefore, the mixture fraction is zero at the vitiated air inlet and is 1 at the fuel inlet.

PSR calculations based on detailed methane kinetics were conducted, and non-equilibrium thermoproperties were produced. Figure 15 shows temperature and concentrations of  $O_2$ ,  $CO_2$ ,  $CO$  and  $NO$

as functions of mixture fraction and residence time, respectively. The blue color region in the temperature plot (Fig. 15a) indicates that the PSR is either in the lean–blow–out state or rich–blow–out state. From the CO plot (Fig. 15d), it is seen that high CO concentration arise in the fuel–rich region.

A 2–D axisymmetric CFD model was built to simulate the combustng flow in the second stage burner. The inlet flow (Feed 1) was assumed to be uniform with certain amount of residual swirl from the first stage burner. The fuel injection was modelled as a point source of mass in the steam of Feed 1. The standard  $k-\epsilon$  model was adopted for turbulent mixing, while the PSR microstructural model was used for combustion.

Table 3 lists the conditions of the case studied.

Table 3. Fuel Staging Combustion – Inlet Conditions to the Second Stage Burner

	Feed 1 – Vitiated Air	Feed 2 – Fuel
Pressure	6.2 atm	6.2 atm
Temperature	1273 K	350 K
Composition in mole fraction	O <sub>2</sub> 13.58% N <sub>2</sub> 76.35% CO <sub>2</sub> 3.36% H <sub>2</sub> O 6.71%	CH <sub>4</sub> 100%
Flow rate	0.434 kg/s	0.0059 kg/s

### 2.4.3 Comparison

**Flow Field** The flow field in the second stage burner can be characterized by jet diffusion and a wake generated from the sudden expansion from the contraction to the combustion chamber. In the center of the rig, a jet stream starts from the fuel injection point. In the first part, the jet diffused into the air stream due to the momentum gradient. As the flow develops downstream, the jet merged with the back–step wake, and then the jet rapidly diffused into the wake and lost its identity. Figure 16 shows contour plots of the axial velocity and turbulent kinetic energy which indicate the development of jet and the wake.

**Mixing of Fuel and Air** The mixing of fuel and air basically follows the jet and wake development described above. Figure 17 is a contour plot of mixture fraction. It is noted that in the first part of jet development, the fuel mixes with air rather slowly. As the jet merged with the wake, the mixing rate increases significantly. The increasing expansion ratio of the mixture fraction contours demonstrate this phenomenon.

**Combustion** The fuel injected in the second stage burner autoignites as it mixed with the vitiated air. A temperature plot (Fig. 18) indicates that the flame starts at about 7.5 cm. downstream from the expansion plane. The first part of the flame has a shape of jet diffusion flame, and as the jet merges with the wake, the flame expanded rapidly and filled the entire cross–section. At the exit of combustor, the temperature profile is flat.

The peak temperature occurs in the region where the mixture fraction is around stoichiometric, which is 0.04 in this case. The peak of the mean temperature (2160 K shown in Fig. 18) is about 200 K less than the adiabatic equilibrium temperature, which is 2350 K, at the stoichiometric mixture fraction. The adiabatic

equilibrium temperature for methane burning in the vitiated air is plotted in Figure 19. It shows that the equilibrium temperature is above 1800 K when the mixture fraction falls between 0.0154 and 0.0772. Using this mixture fraction range as plotting threshold, the mean temperature in this case changed from 1700 K to 2160 K shown in Figure 20. Because of the relatively low flame temperature, the NO formation is expected to be low. Figure 21 shows that the NO produced in the second stage burner amounts to only a few ppm (at the exit of the burner).

To explain how low NO<sub>x</sub> is achieved in this diffusion-type flame, we need to take a close look at the kinetic effect and the interaction of mixing and kinetics. Figure 22 is a contour plot of the mean residence time. It is shown that in the first part of flame, i.e., in the diffusion-type flame, because of high strain rate, the residence time is so small that the flame is basically in a non-equilibrium state. In the second part of the flame, strong turbulent mixing occurs, and the residence time increases as well. However, because of large fluctuations of turbulence and scalars, the PDF of the residence time and the PDF of the mixture fraction are flat. As a result, the mean temperature in this region, which is determined from a wide spectrum of mixture fraction and residence time, is much lower than the temperature determined from the mean values of mixture fraction and residence time. To illustrate this feature, flame properties at two locations in the hot temperature zone are selected and listed in Table 4. At these two locations, although the mean mixture fraction is close to stoichiometric value, the standard deviation (the square root of  $g$ ) is large, which results in a low mean temperature. The same argument is found in terms of the residence time.

Table 4. PDFs of mixture fraction and residence time in the flame zone

	mean mixture fraction	standard deviation of mixture fraction	mean residence time	standard deviation of $\ln\tau$	mean temperature	equilibrium temperature
Location 1	0.038	0.0187	1.2ms	1.0	2160K	2352K
Location 2	0.031	0.0155	1.3ms	1.0	2117K	2240K

**Comparison with Test Results** Measured data are available at the exit of the second stage burner. Table 5 shows a comparison in terms of concentrations of O<sub>2</sub>, CO<sub>2</sub> and NO, with good agreement.

Table 5. Comparison of test data and CFD results

	Test Data	CFD Results
Mole Fraction		
O <sub>2</sub>	0.086	0.083
CO <sub>2</sub>	0.055	0.056
NO	6ppm	3ppm

#### 2.4.4 Conclusions from Application to High-Pressure Staged Combustor

The PSR microstructural model was applied to staged combustion, where mixing and chemical kinetic effects on ignition are important. NO<sub>x</sub> is lower than in a conventional one-stage combustor. The PSR microstructural model was successful in calculating significant features of this combustor.

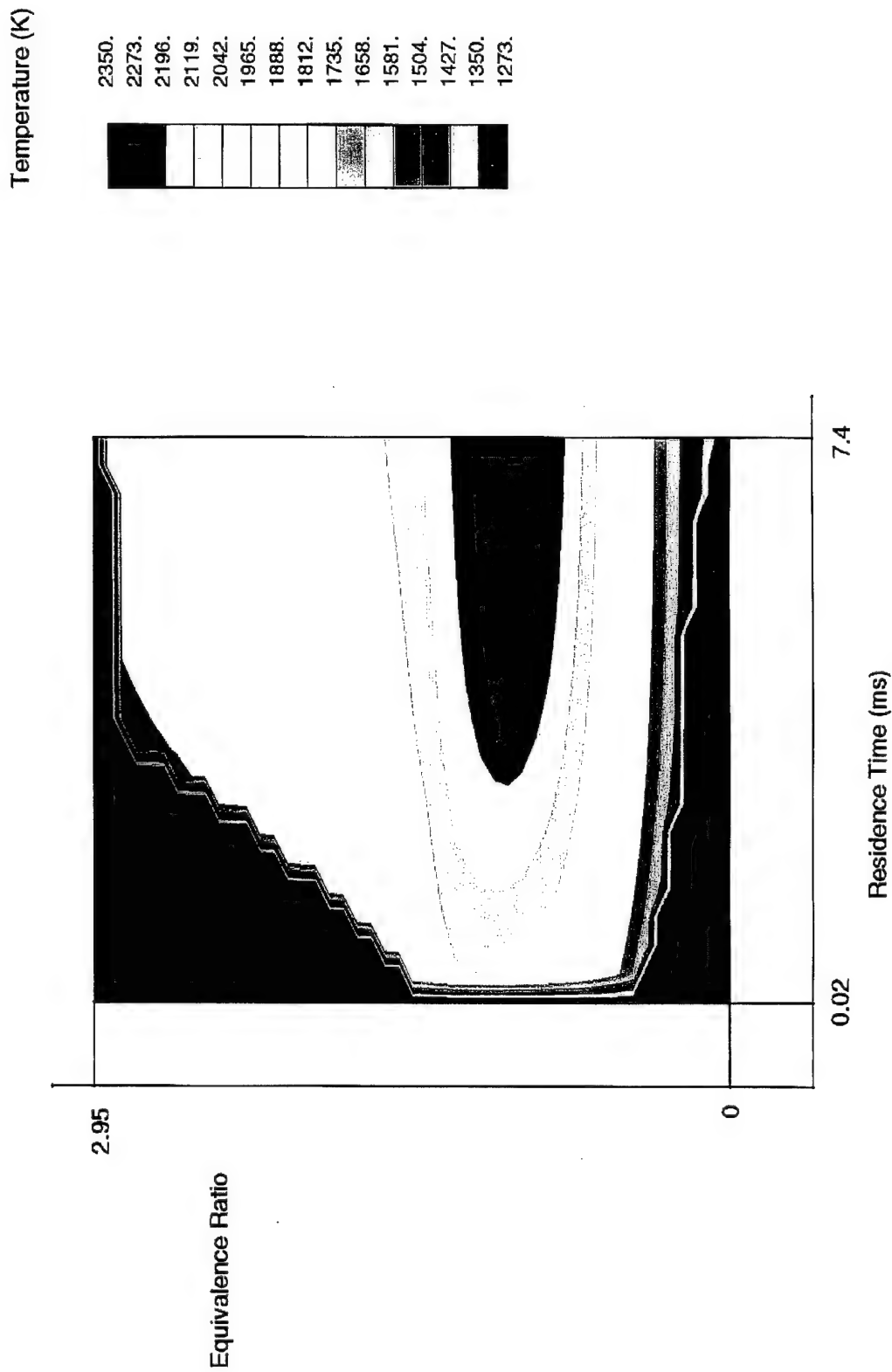


Figure 15a. PSR thermoproperties of methane burning in vitiated air (Inlet 6.2 atm, 1273K).  
Temperature

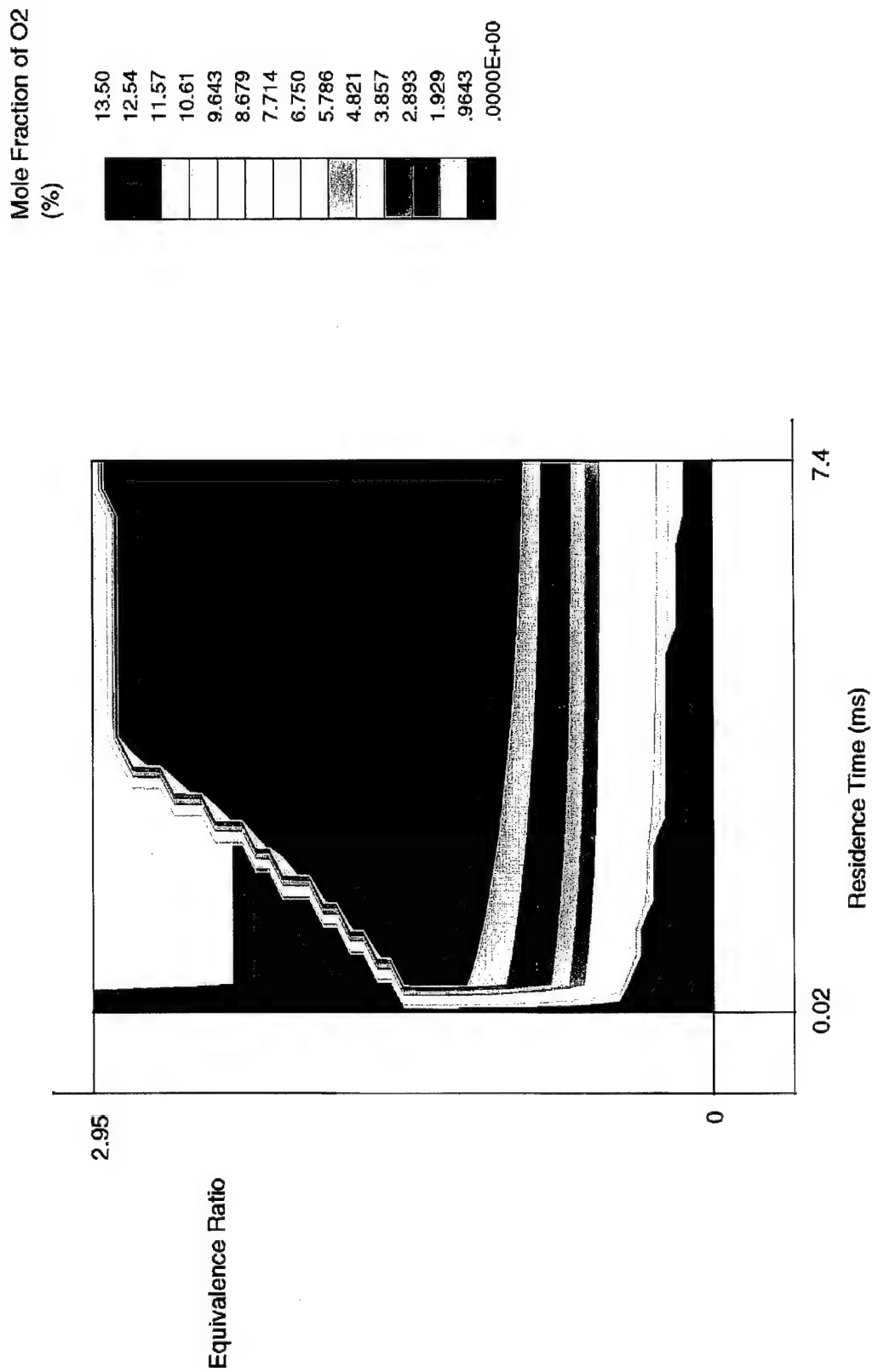


Figure 15b. PSR thermoproperties of methane burning in vitiated air (Inlet 6.2 atm, 1273K).  
Mole fraction of O<sub>2</sub>.

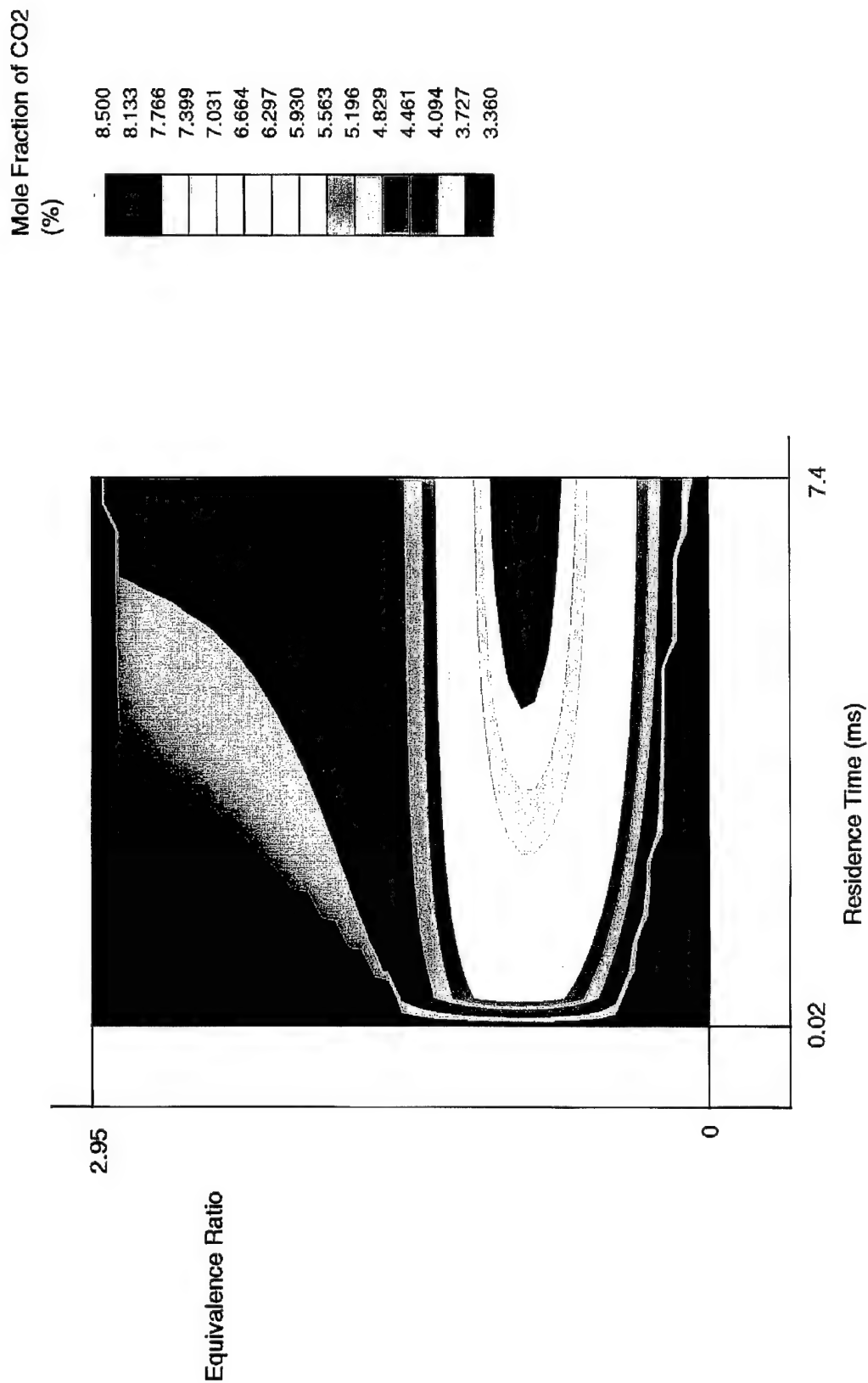


Figure 15c. PSR thermoproperties of methane burning in vitiated air (Inlet 6.2 atm, 1273K).  
Mole fraction of CO<sub>2</sub>.

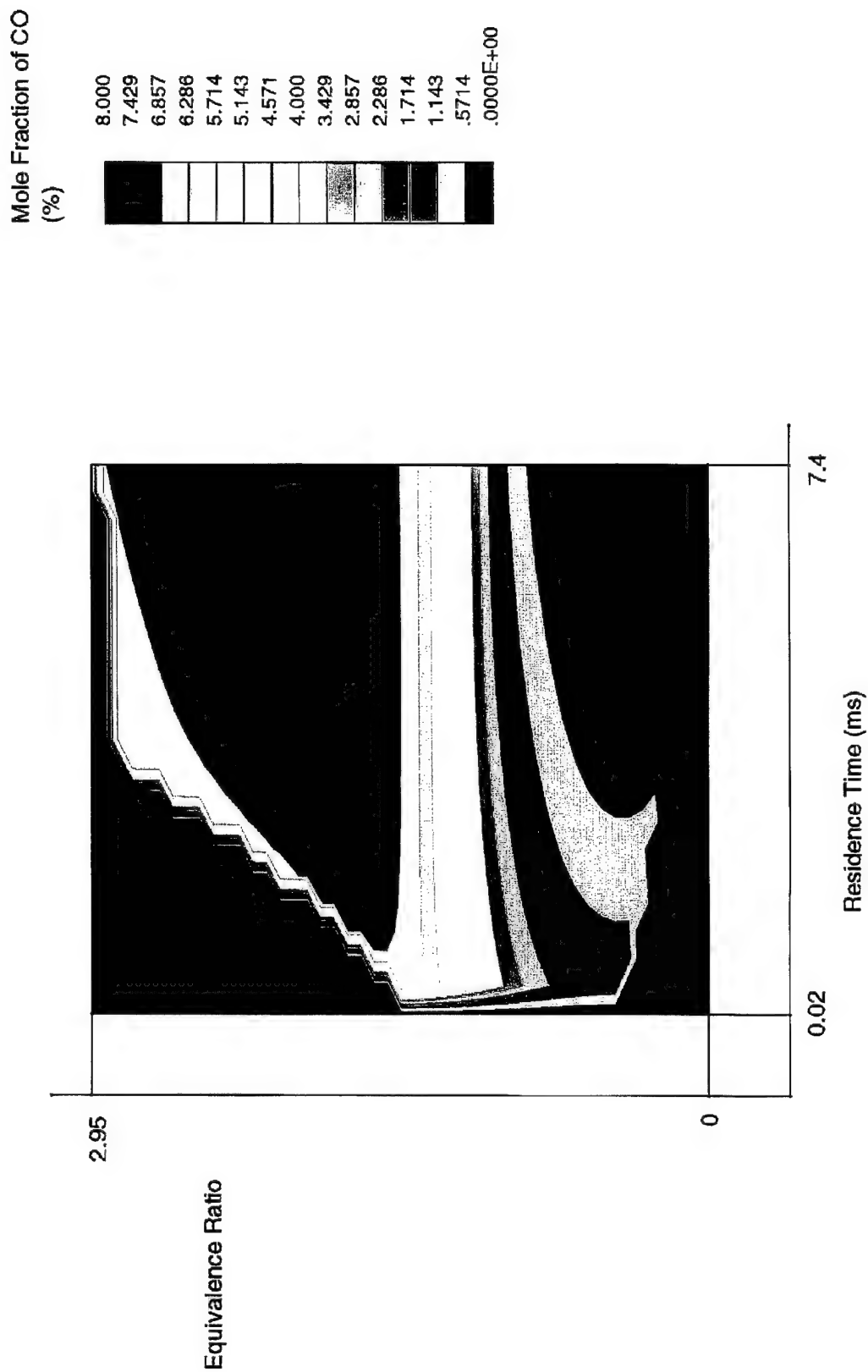


Figure 15d. PSR thermoproperties of methane burning in vitiated air (Inlet 6.2 atm, 1273K).  
Mole fraction of CO

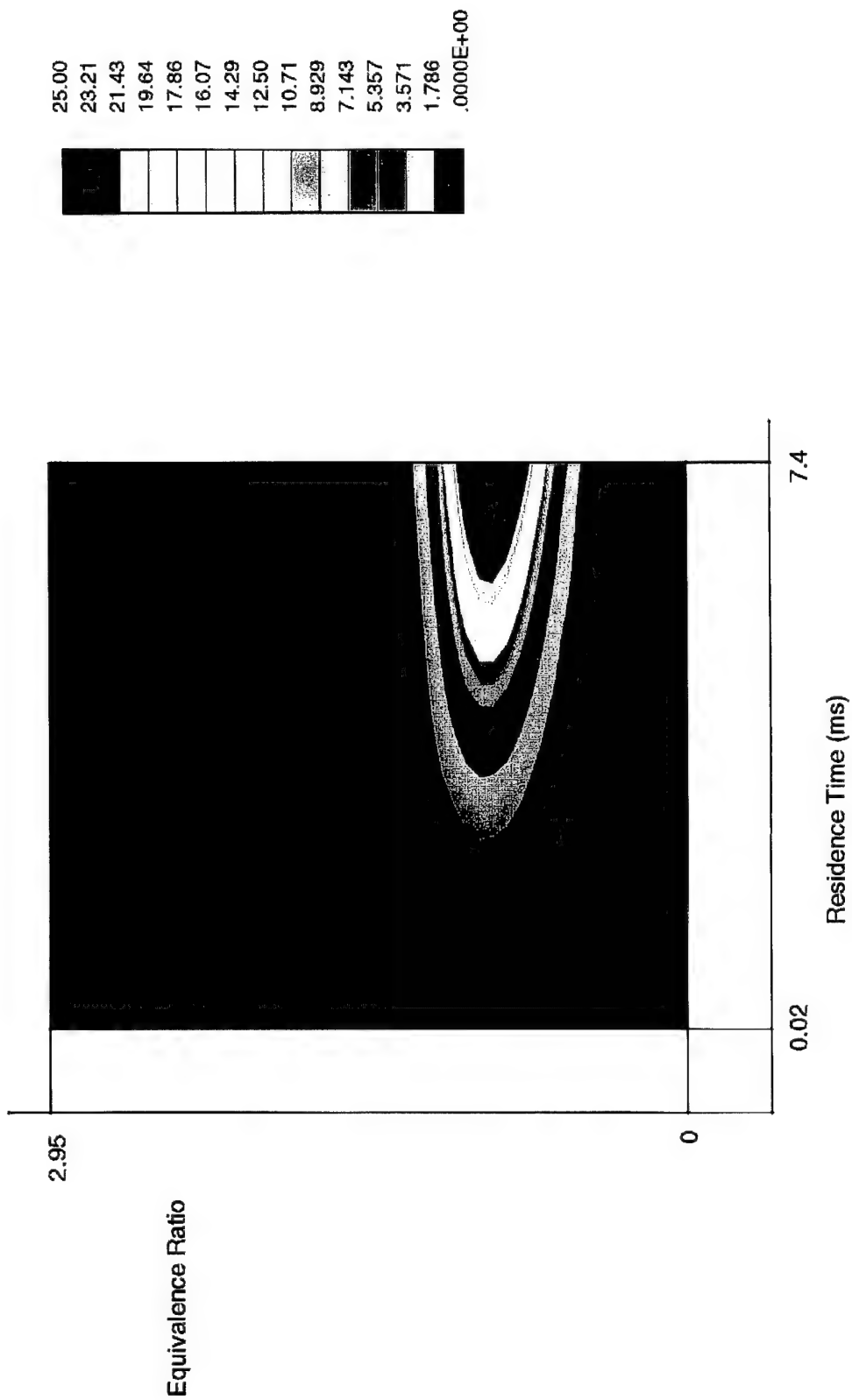


Figure 15e. PSR thermoproperties of methane burning in vitiated air (Inlet 6.2 atm, 1273K).  
Mole fraction of NO.

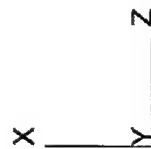
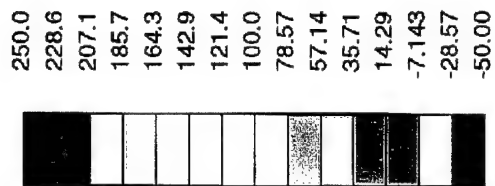


Figure 16a. Calculation of second burner in fuel staging rig.  
Axial velocity (M/S).

2000.  
1857.  
1714.  
1571.  
1429.  
1286.  
1143.  
1000.  
857.1  
714.3  
571.4  
428.6  
285.7  
142.9  
.0000E+00

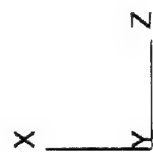


Figure 16b. Calculation of second burner in fuel staging rig.  
Turbulence kinetic energy distribution ( $M^2/S^2$ ).

.1200  
 .1114  
 .1029  
 .9429E-01  
 .8571E-01  
 .7714E-01  
 .6857E-01  
 .6000E-01  
 .5143E-01  
 .4286E-01  
 .3429E-01  
 .2571E-01  
 .1714E-01  
 .8571E-02  
 .0000E+00



X  
 Y Z

Figure 17. Mixture fraction distribution in the second burner.

2160.  
2097.  
2033.  
1970.  
1907.  
1843.  
1780.  
1717.  
1653.  
1590.  
1526.  
1463.  
1400.  
1336.  
1273.

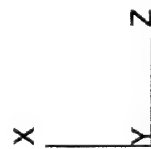


Figure 18. Mean temperature distribution in the second burner (K).

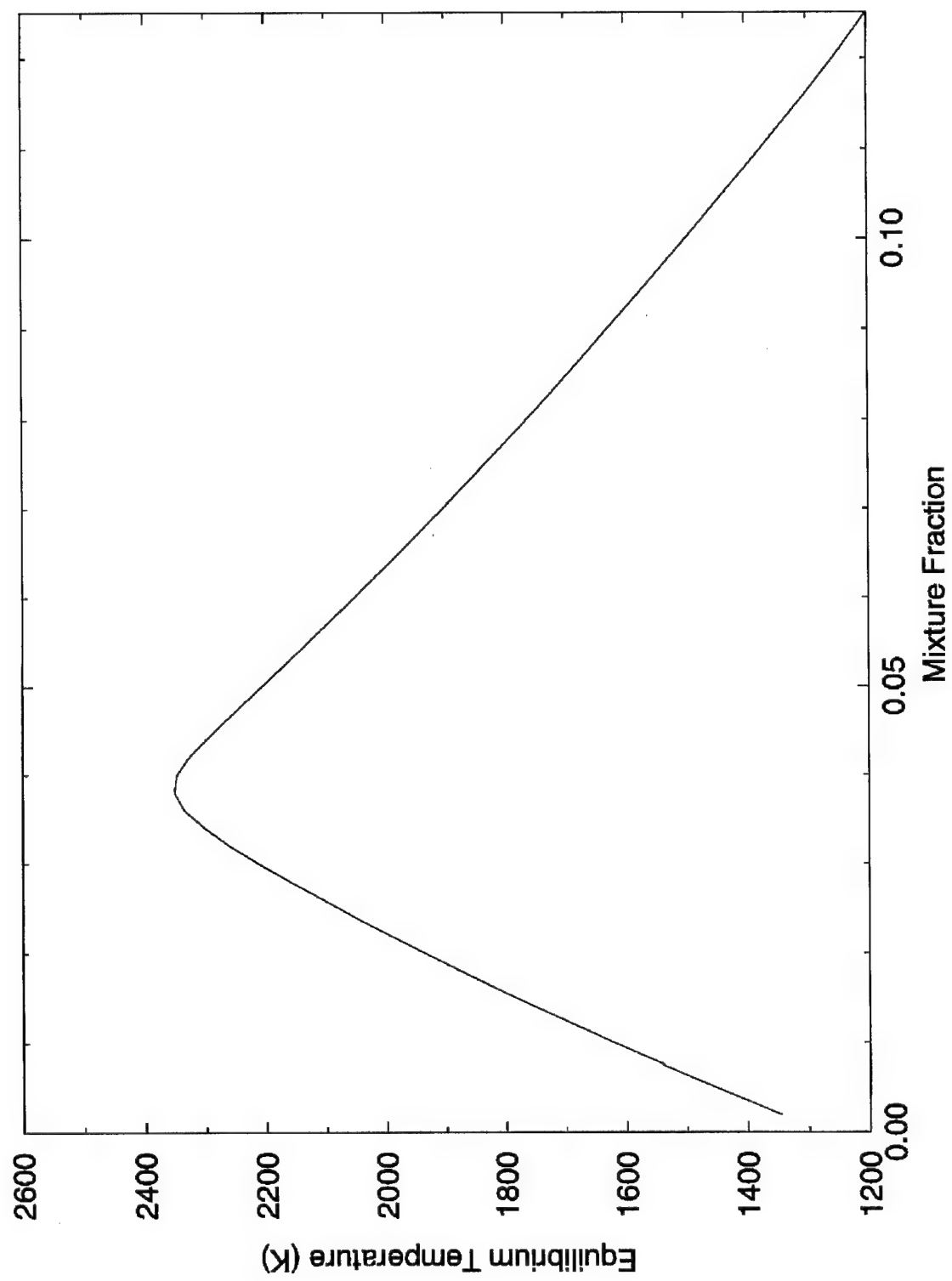


Figure 19. Adiabatic equilibrium temperature of methane combustion in vitiated air (Inlet 1273K).

2160.  
2097.  
2033.  
1970.  
1907.  
1843.  
1780.  
1717.  
1653.  
1590.  
1526.  
1463.  
1400.  
1336.  
1273.

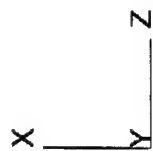


Figure 20. Temperature distribution in the (mean) mixture fraction range of 0.0154 and 0.0772 (K).

25.00  
23.21  
21.43  
19.64  
17.86  
16.07  
14.29  
12.50  
10.71  
8.929  
7.143  
5.357  
3.571  
1.786  
.0000E+00

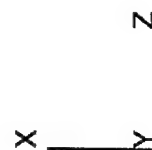


Figure 21. NO distribution in the second burner (ppm).

5.000  
4.643  
4.286  
3.929  
3.571  
3.214  
2.857  
2.500  
2.143  
1.786  
1.429  
1.071  
.7143  
.3571  
.0000E+00

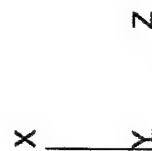


Figure 22. Mean residence time distribution in the second burner (ms).

## 2.5 Aircraft Engine Combustor

A can-type combustor which was scaled from a Tay engine was used for combustion measurements under the engine take-off condition [Bicen et al. (1990)]. The combustor was fueled with gaseous propane at the atmospheric pressure. Combustion quantities, such as temperature and concentrations of major species, were collected in the flame zone within the combustor by using small-diameter bare-wire thermocouples and sampling probes. This combustion case is of interest to us because its configuration is similar to a real engine combustor and the test data consist of flame property maps inside combustor. In addition, this combustion case used propane fuel which features more complicated chemical kinetics than methane. Therefore, this combustion case is used as a test of the PSR microstructural model in a more practical environment.

### 2.5.1 Experimental Set-Up

Figure 23 shows the arrangement of the combustor. The inlet part of the combustor includes a fuel injector and a swirler. The burner part of the combustor consists of a hemispherical head section, a circular can section and a circular-to-rectangular nozzle section. The inner and outer annular diameters of the swirler are 15 mm and 40 mm, respectively. The experiment showed that the discharge swirl number is 0.56. Fuel is introduced from ten small jets spaced circumferentially around a  $90^\circ$  cone located at the center of the swirler. The diameter of the fuel jets is 1.7 mm. The diameter of the burner can is 75 mm. The burner contains a set of six primary holes of 10 mm in diameter and a set of six dilution holes of 20 mm in diameter which located 80 mm downstream from the primary holes. The dilution holes are staggered by half a pitch with respect to the primary holes. Detailed dimensions can be found in the references [Bicen et al. (1990); Bicen and Jones (1986)].

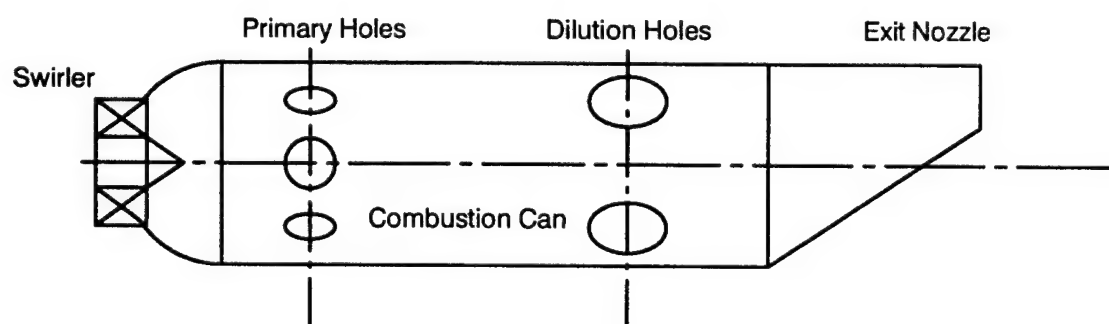


Figure 23. Sketch of the can-type combustor.

The combustion test was conducted with an inlet temperature at 315 K. To simulate an engine take-off condition, the amount of air coming from the swirler is relatively small, which creates a fuel-rich zone before the primary air injection. The primary holes were designed in such a way that the primary jets impinged and part of primary air flowed upstream and contributed to the primary recirculation.

### 2.5.2 Thermoproperties of Propane in a PSR

A detailed kinetic scheme for propane [Konnov (1997)], which contains 996 reaction steps and 121 species, was used in the PSR calculations. The thermoproperties of propane combustion in a PSR, which are characterized by mixture fraction and residence time, are shown in Figure 24.

### 2.5.3 CFD Model

A 3-D CFD model for the entire can was built. The model uses the multi-block meshing feature of the CFD code and has a total number of 60,000 cells. Since only the flame properties in the primary zone were of interest, the exit nozzle was not modelled in detail but the exit cross-sectional area was used. In the CFD model, the turbulence was modelled by the standard  $k-\epsilon$  model and the combustion was modeled by the PSR microstructural model.

The inlet flow was assumed to be uniform. Velocities at different inlets were determined from the flow rates and were assumed to be perpendicular to the inlet surfaces, except at the swirler inlet where the velocity components were determined from the Swirl Number. It was found that the flow pattern in the primary zone was very sensitive to the flow split. The suggested flow split in the paper of Bicen et al. [1990] did not result in a flow pattern shown in their paper. In order to achieve a more realistic flow pattern and test the PSR model, the flow split was adjusted as follows. The air emitted from the transply head and transply can were removed and redistributed among the primary holes, dilution holes and transply nozzle. The resulting flow splits are: swirler – 6.9%, primary holes – 15.3%, dilution holes – 60%, nozzle – 17.8%.

### 2.5.4 Comparison

In this case the PSR microstructural model is only applicable to the primary reaction zone. In the following, modeling results are analyzed and compared with the test data in the primary zone only. Results are plotted in the mid-horizontal plane and in the mid-vertical plane (where the test data are available). The CFD results are presented in color contour plots, while the test results are included in a line contour format.

The flow pattern is shown by velocity vectors in the mid-horizontal plane (Fig. 25a) and in the mid-vertical plane (Fig. 25b). It is shown that there are two symmetric vortices in the primary zone, which result from the swirling inlet condition. In the center of the combustor, the flow is reversed. It is also shown that the primary air jets penetrate deeply and impinge at the center of the combustor. Some amount of primary air flows reversely and participates the primary recirculation. This flow pattern is similar to the pattern described in the paper [Bicen et al. (1990)].

The calculated equivalence ratio field is shown in Figs. 26 and 27, along with the test data. It is seen that the equivalence ratio contours in the primary zone are similar between the CFD calculations and the test data. Additional quantities are compared in Figs. 28–35, again with generally good agreement between calculations and measurements.

To demonstrate the chemical kinetic effect and interaction of mixing and kinetics, the PDF parameters at two locations are listed in Table 5. These two locations are in the center of the primary recirculation zone. At both locations, the mean residence time is above 10 ms, which indicates that the flame is at equilibrium state in the mean sense. However, because of large fluctuations of scalars – which are shown by the large deviations from the mean – the mean temperature is much lower than the equilibrium temperature at the same equivalence ratio.

Table 5. PDF parameters in the center of primary zone

	mean mixture fraction	standard deviation of mixture fraction	mean residence time	standard deviation of $\ln \tau$	mean temperature	equilibrium temperature
Location 1	0.075	0.0275	11 ms	0.543	1600K	2090K
Location 2	0.089	0.0275	11 ms	0.516	1550K	1920K

### 2.5.5 Conclusions from Application to Practical Combustor

The PSR microstructural model was applied to a practical combustion configuration where the flame is stabilized in a swirling flow and the combustor is fueled with a more complex hydrocarbon. It was found that the accuracy of combustion calculation depends on the accuracy of the flow pattern prediction. Given a reasonable prediction of the flow pattern, the PSR microstructural model yielded a good results comparing with the test data. This application has demonstrated the capability of the PSR model in modeling the kinetic effect in a highly turbulent flow regime.

Temperature (K)

2285.  
2144.  
2004.  
1863.  
1722.  
1581.  
1441.  
1300.  
1159.  
1019.  
877.9  
737.1  
596.4  
455.7  
315.0

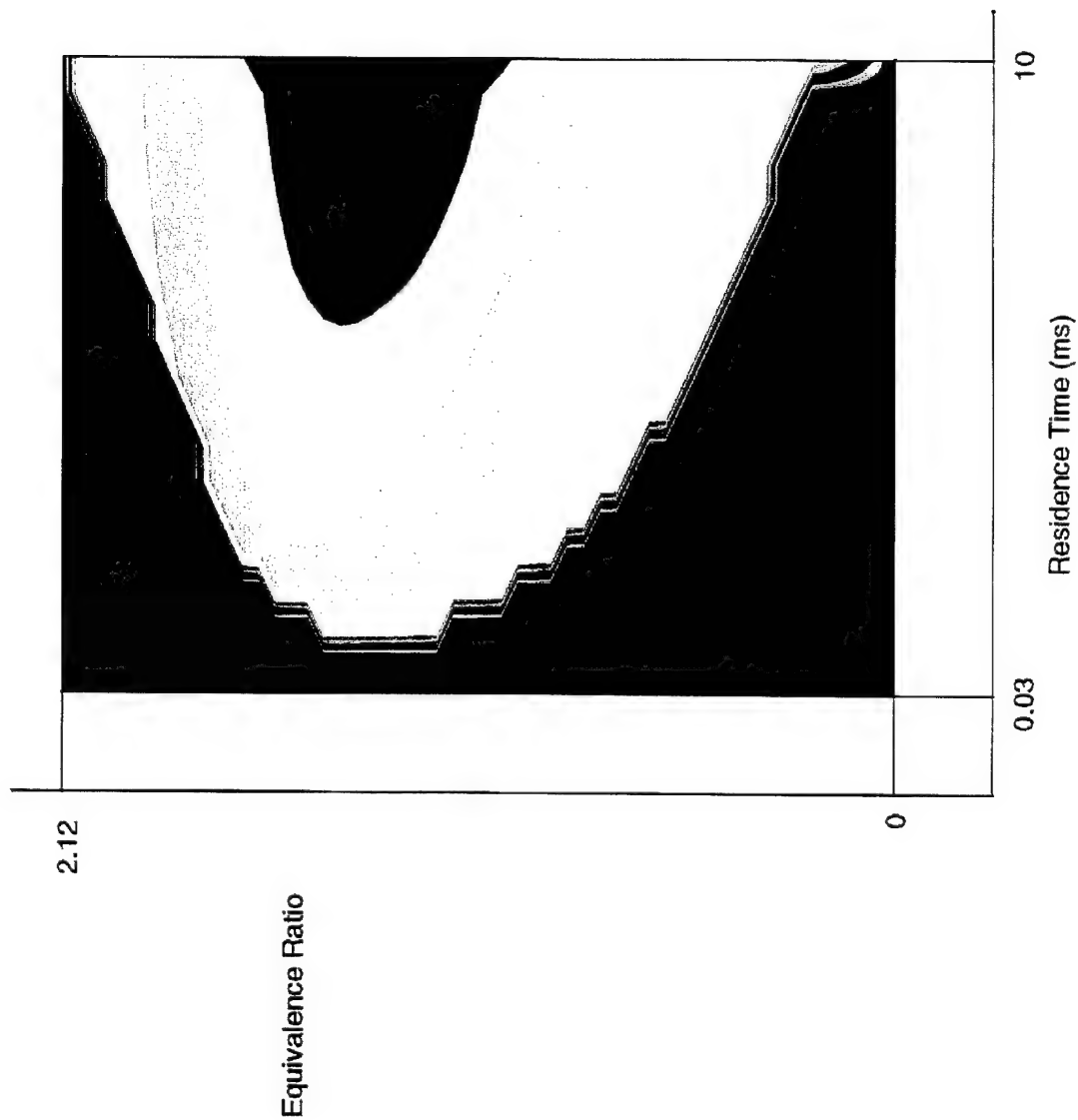


Figure 24a. PSR thermoproperties of propane combustion in air. Temperature.

Mole Fraction of CO<sub>2</sub>  
(%)

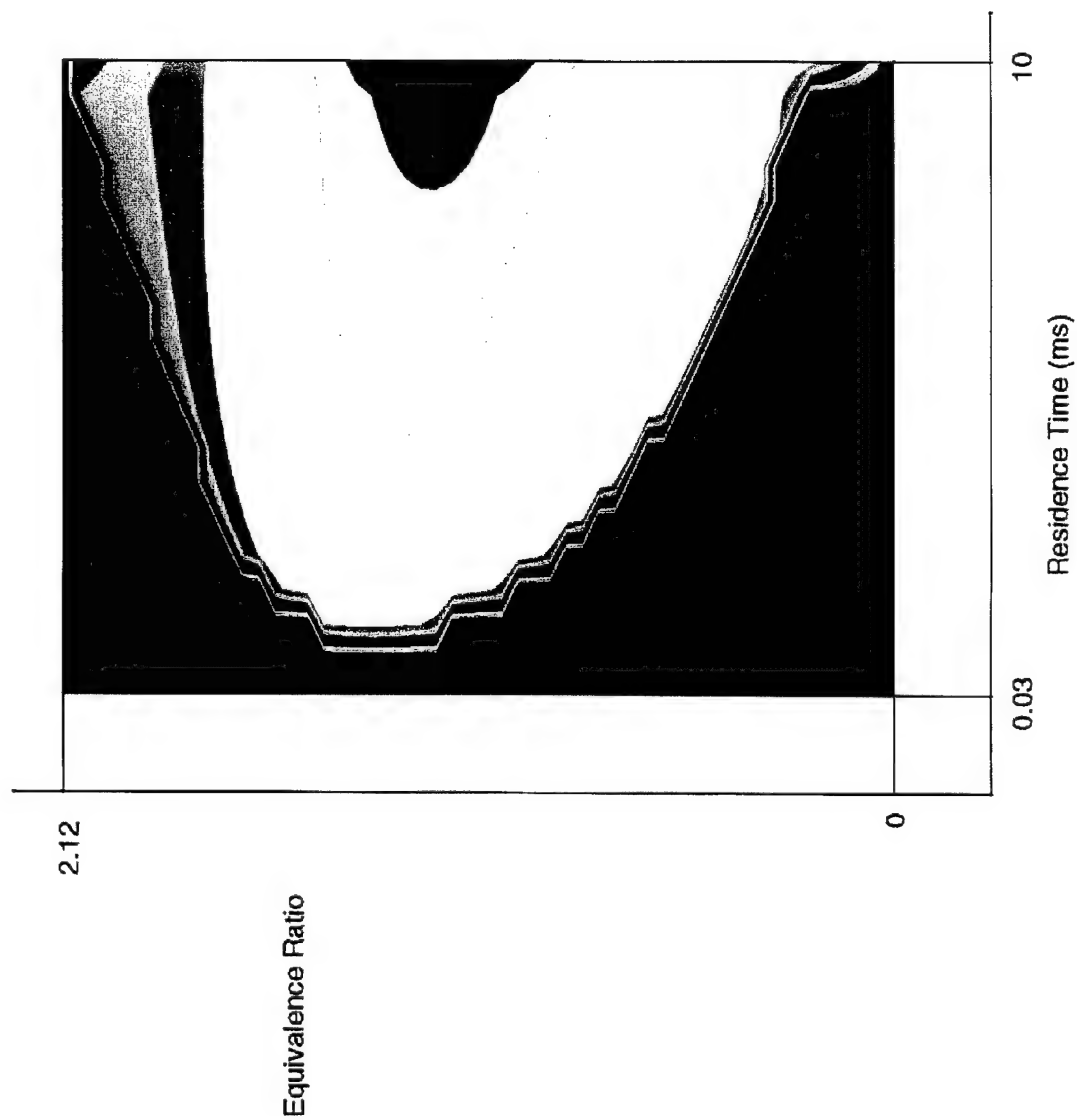
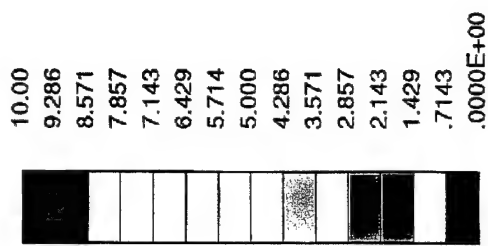


Figure 24b. PSR thermoproperties of propane combustion in air.  
Mole fraction of CO<sub>2</sub>.

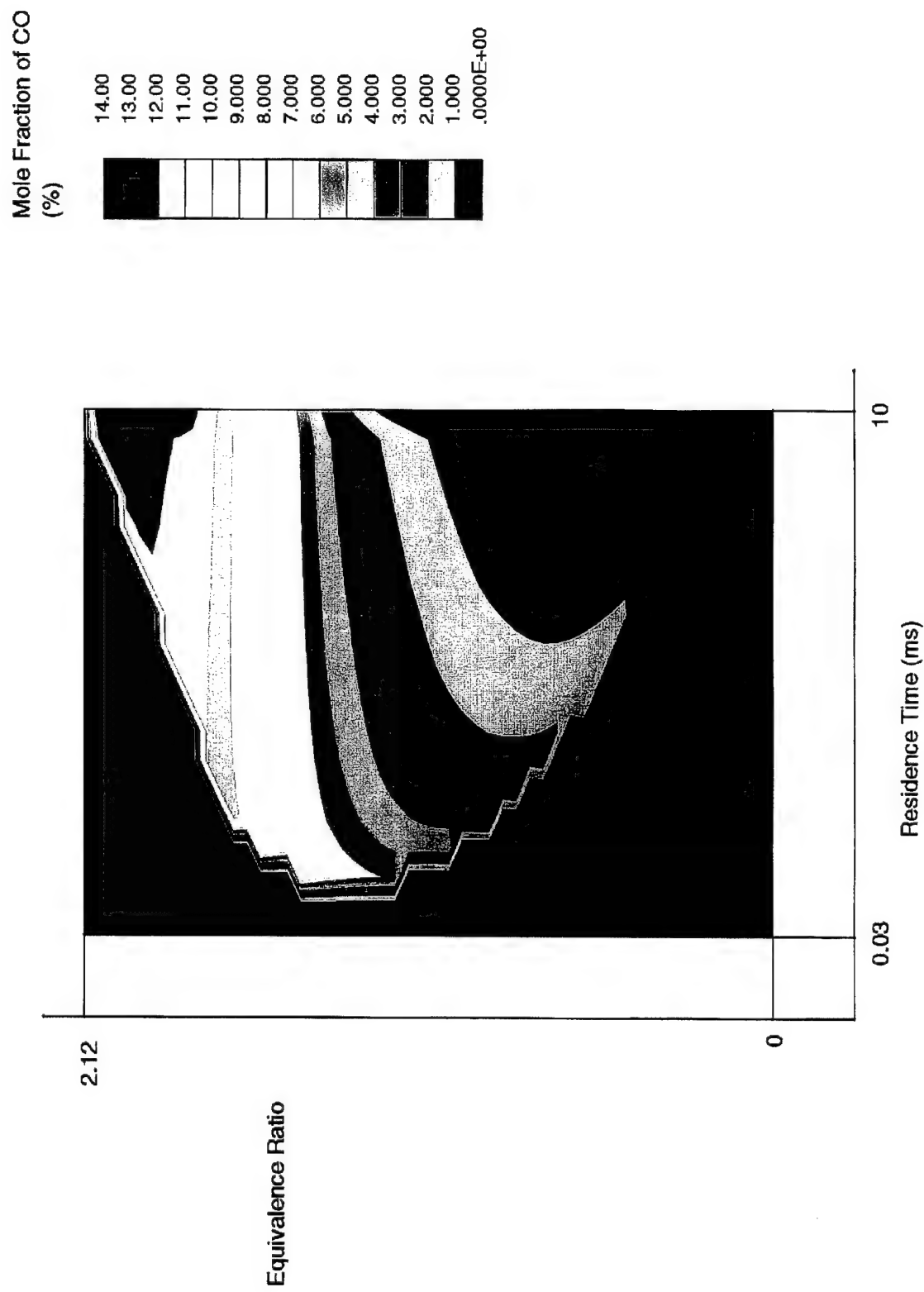


Figure 24c. PSR thermoproperties of propane combustion in air.  
Mole fraction of CO.

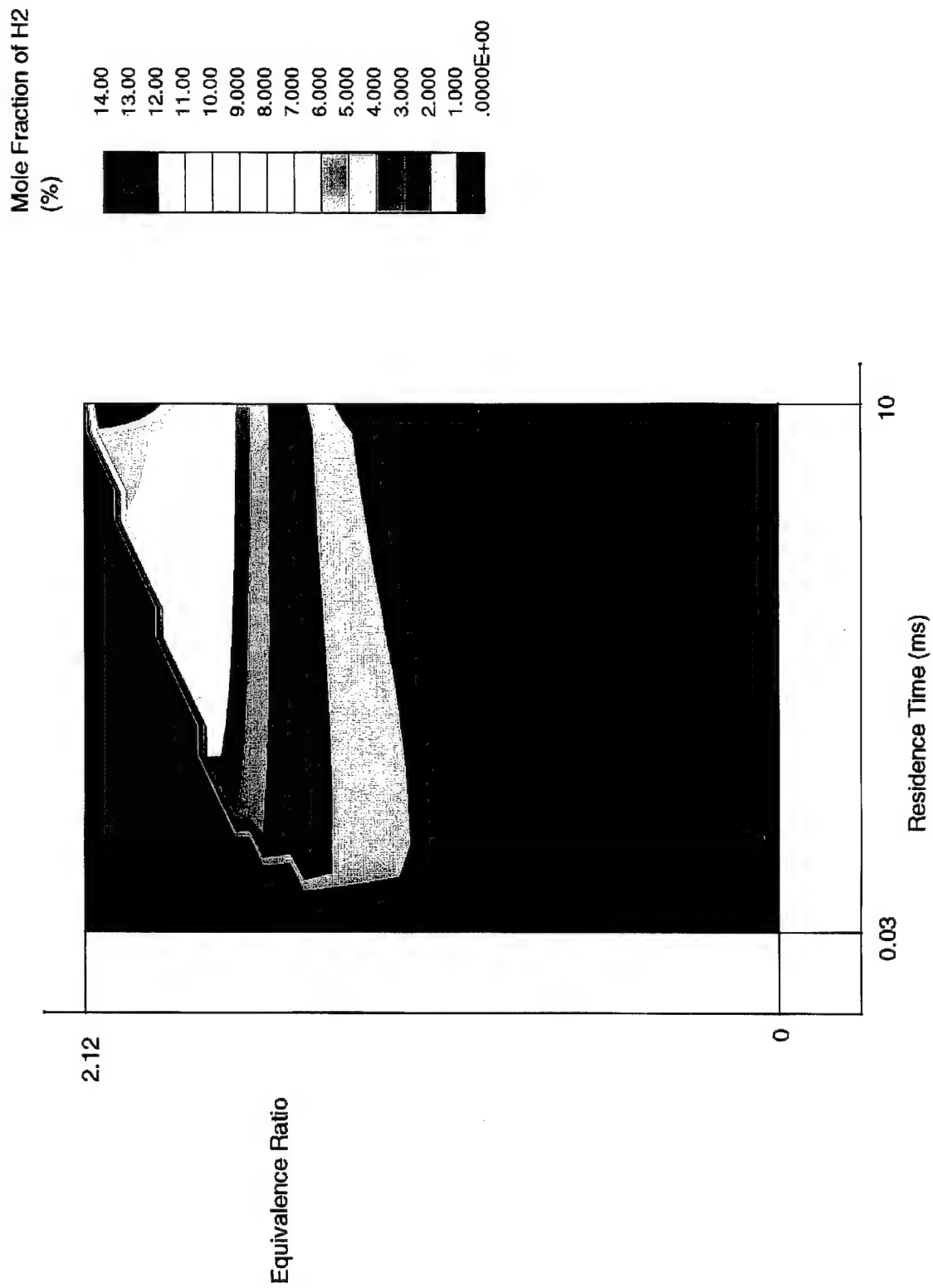


Figure 24d. PSR thermoproperties of propane combustion in air.  
Mole fraction of  $H_2$ .

LOCAL MX= 39.89  
 LOCAL MN= .0000E+00

30.50
28.32
26.14
23.96
21.79
19.61
17.43
15.25
13.07
10.89
8.714
6.536
4.357
2.179
.0000E+00

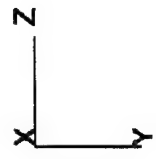
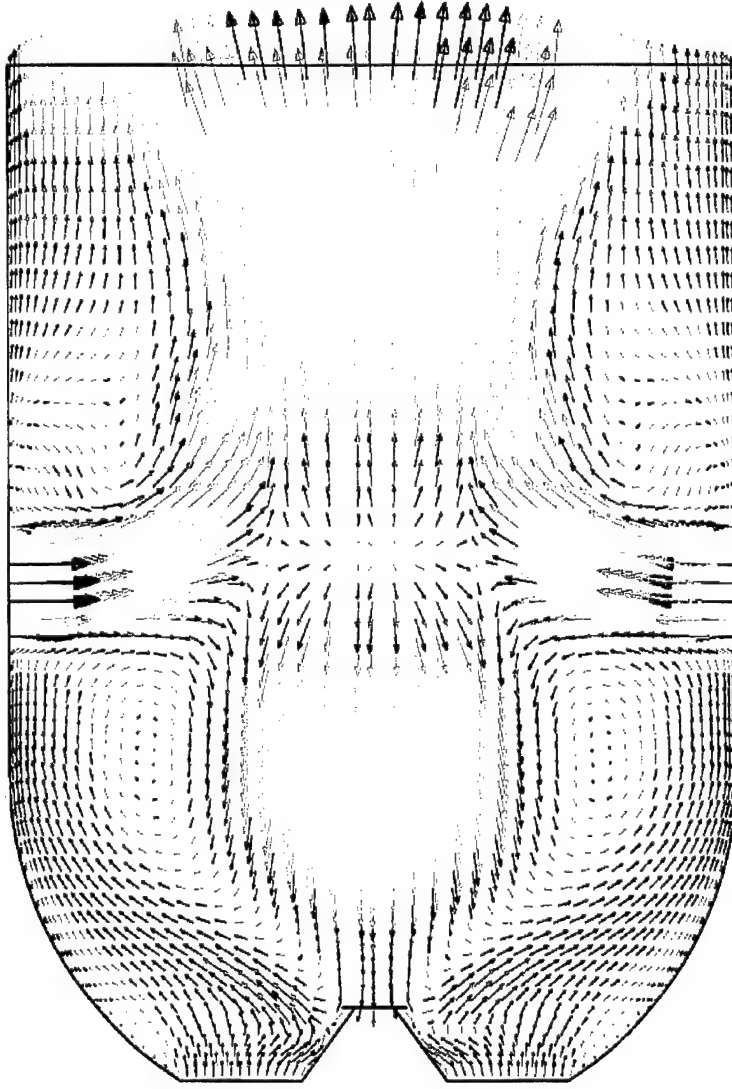


Figure 25a. Velocity vectors in the primary combustion zone (m/s)  
 Mid-horizontal plane.

LOCAL MX= 39.37  
 LOCAL MN= .0000E+00

30.50
28.32
26.14
23.96
21.79
19.61
17.43
15.25
13.07
10.89
8.714
6.536
4.357
2.179
.0000E+00

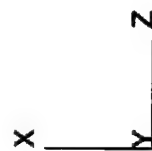
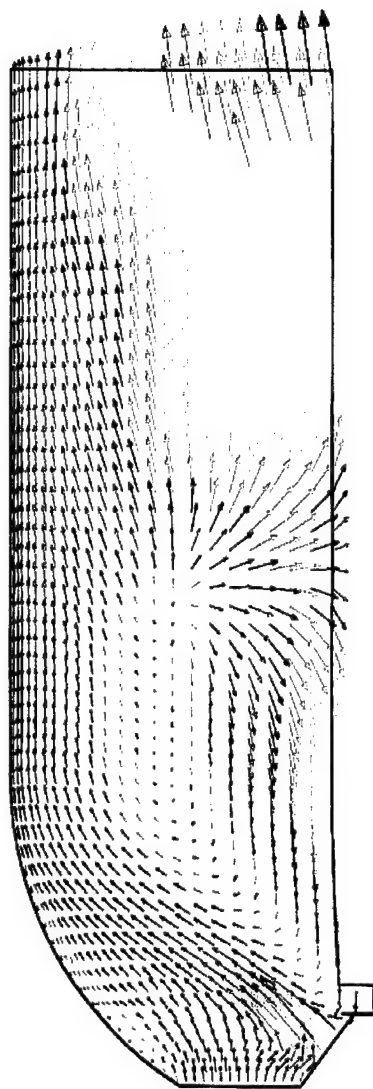


Figure 25b. Velocity vectors in the primary combustion zone (m/s)  
 Mid-vertical plane.

LOCAL MX= 11.72  
LOCAL MN= -.9565E-06

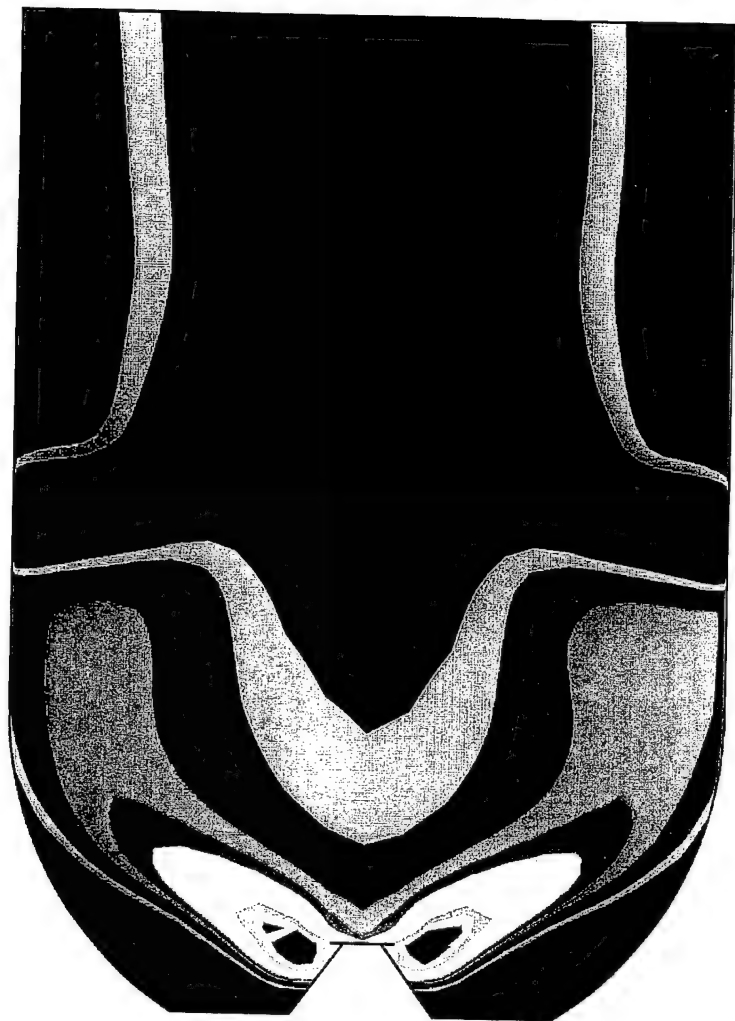
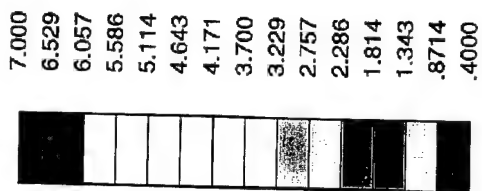


Figure 26a. Distribution of equivalence ratio in the mid-horizontal plane.  
CFD results.

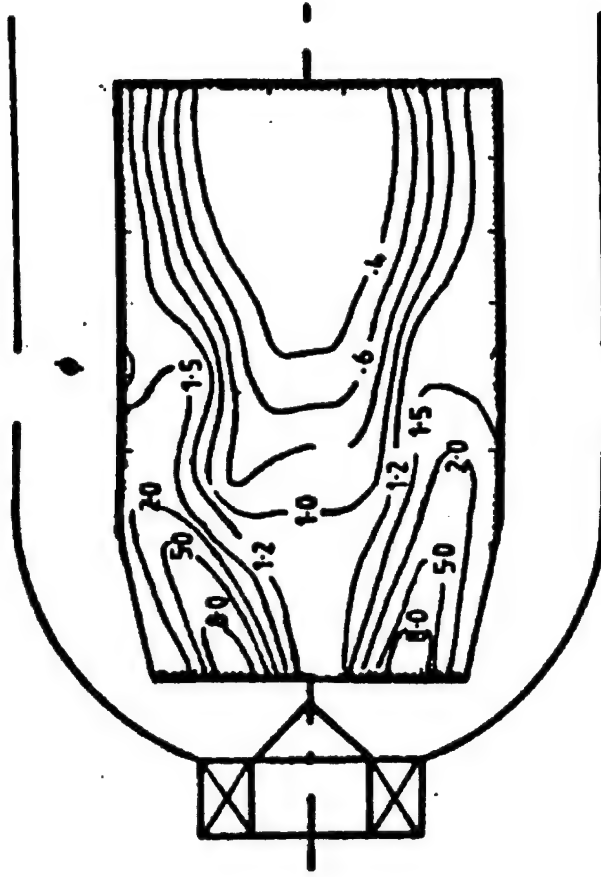


Figure 26b. Distribution of equivalence ratio in the mid-horizontal plane.  
Test results.

LOCAL MX= 11.72  
 LOCAL MN= .0000E+00

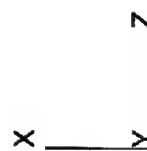
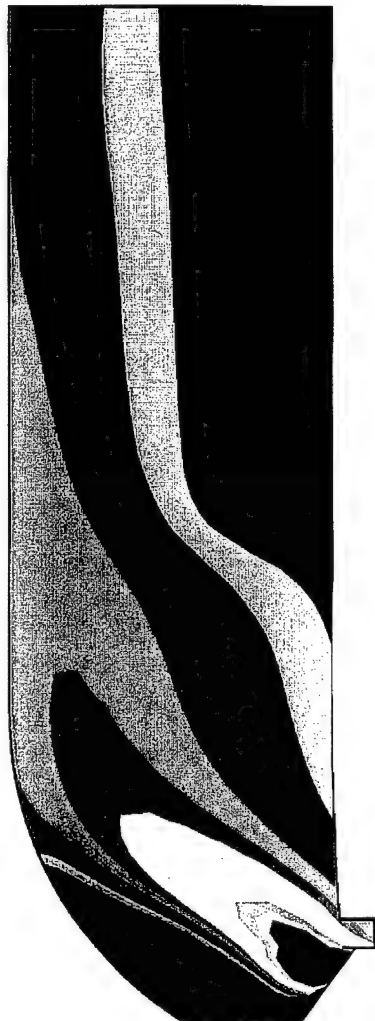
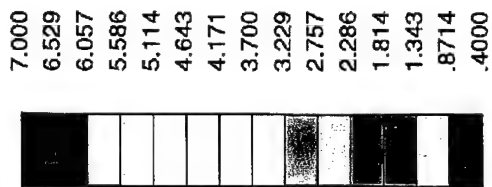


Figure 27a. Distribution of equivalence ratio in the mid-vertical plane.  
 CFD results.

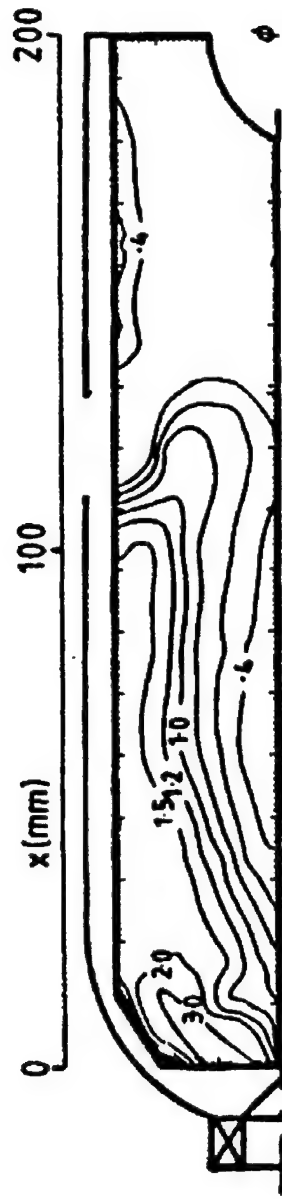


Figure 27b. Distribution of equivalence ratio in the mid-horizontal plane.  
Test results.

LOCAL MX= 2068.  
 LOCAL MN= .0000E+00

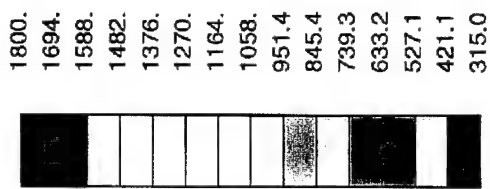


Figure 28a. Distribution of temperature in the mid-horizontal plane (K).  
 CFD results.

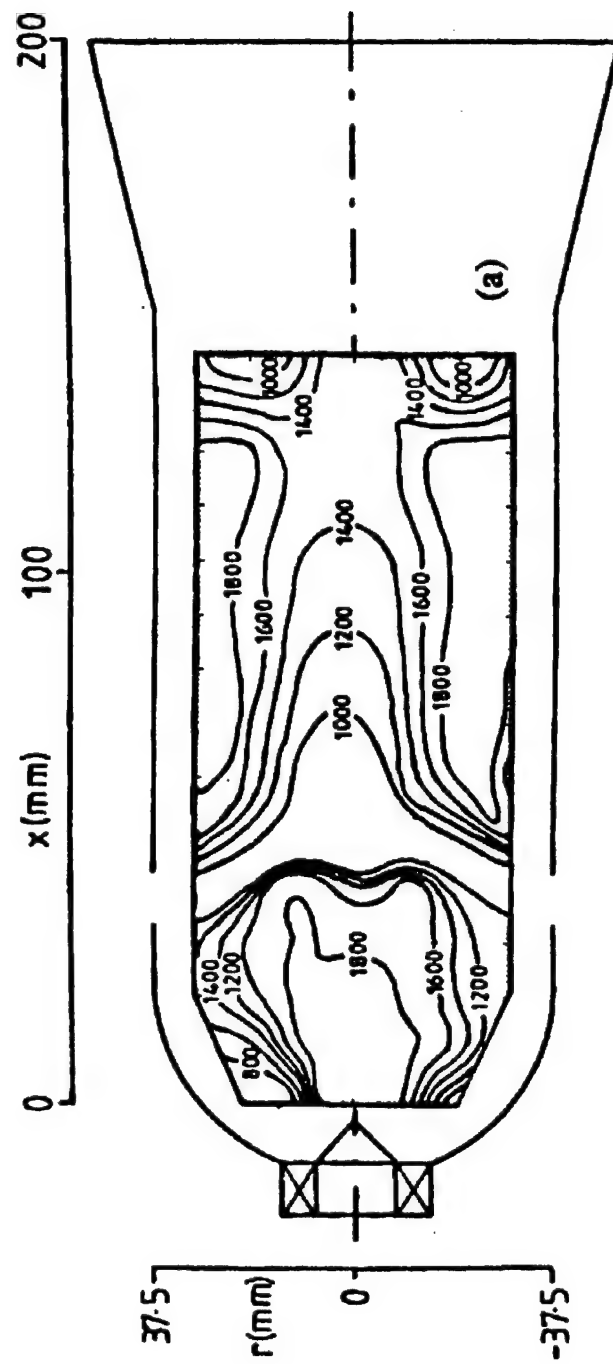


Figure 28b. Distribution of temperature in the mid-horizontal plane (K).  
Test results.

LOCAL MX= 2035.  
 LOCAL MN= .0000E+00

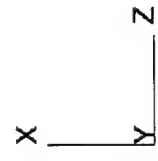
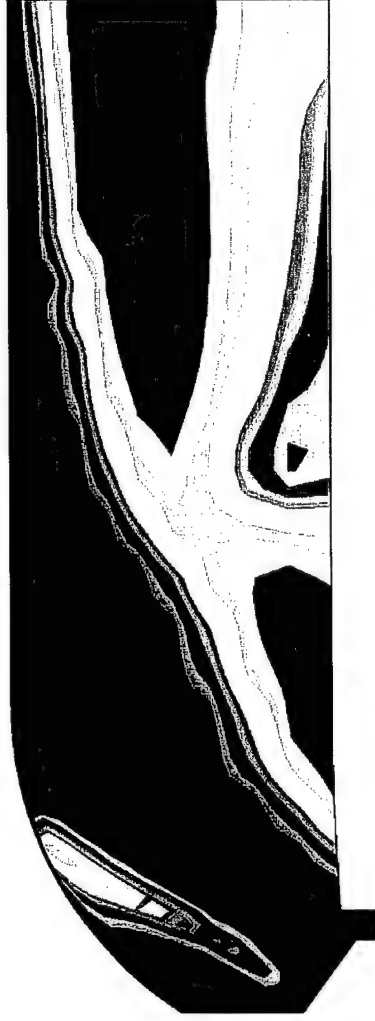
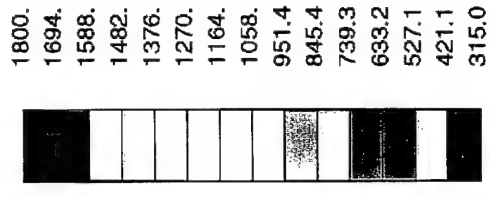


Figure 29a. Distribution of temperature in the mid-vertical plane (K).  
 CFD results.

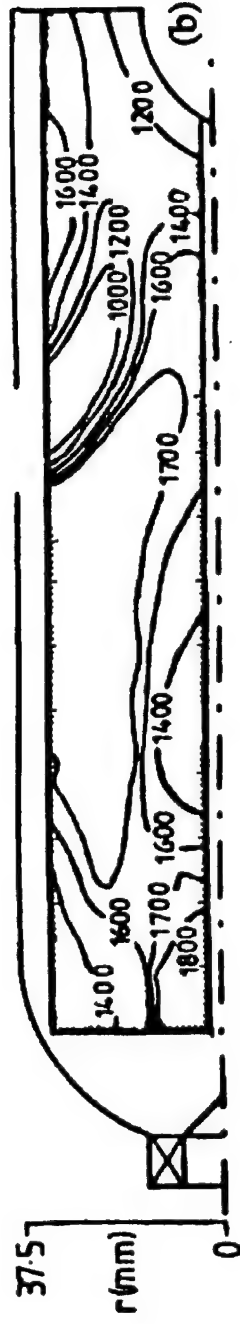


Figure 29b. Distribution of temperature in the mid-vertical plane (K).  
Test results.

LOCAL MX= 15.28  
LOCAL MN= -.6522E-08

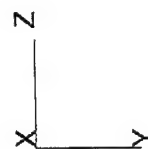
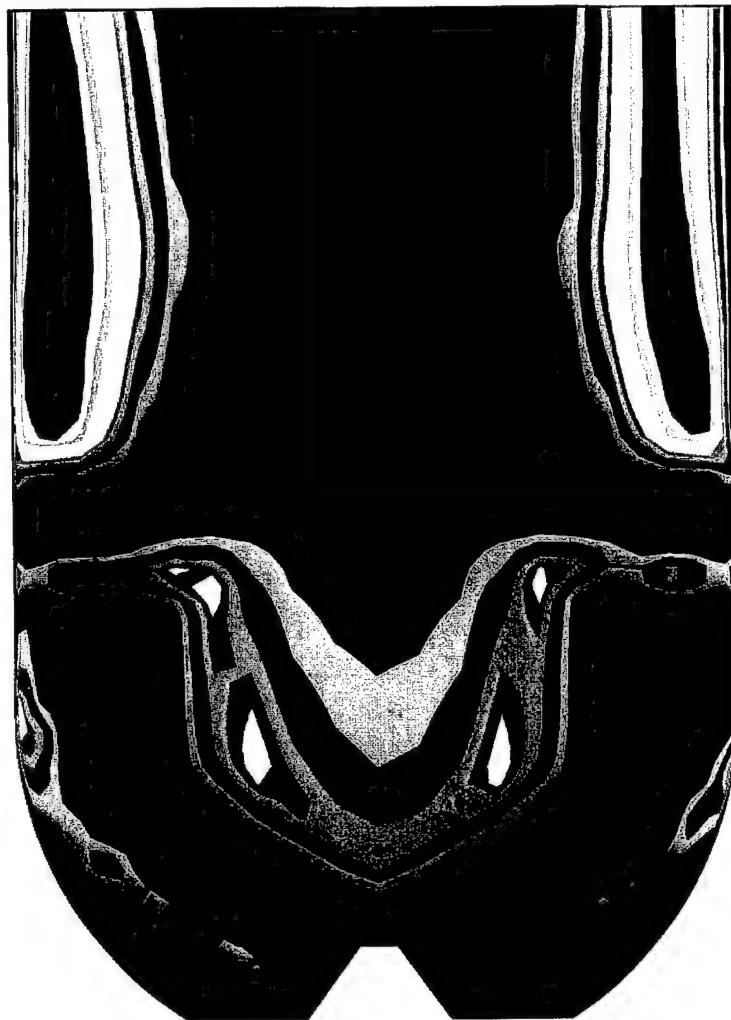
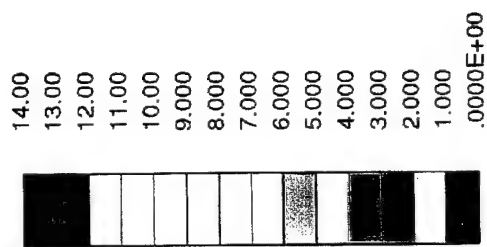


Figure 30a. Distribution of CO concentration in the mid-horizontal plane (mole fraction, %).  
CFD results.

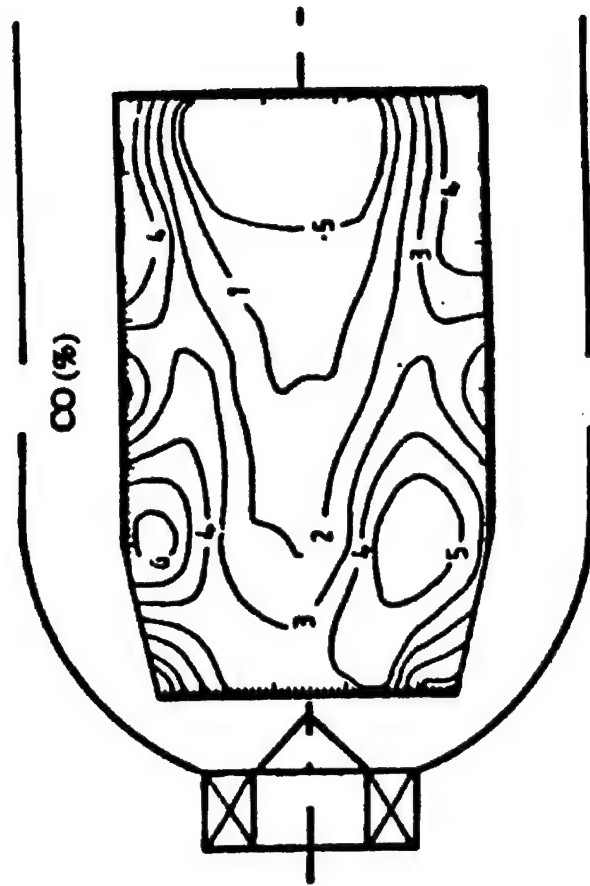


Figure 30b. Distribution of CO concentration in the mid-horizontal plane (mole fraction, %).  
Test results.

LOCAL MX= 13.97  
LOCAL MN= .0000E+00

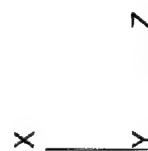
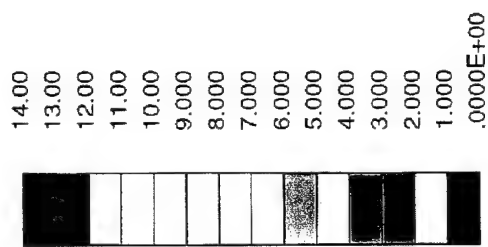


Figure 31a. Distribution of CO concentration in the mid-vertical plane (mole fraction, %).  
CFD results.

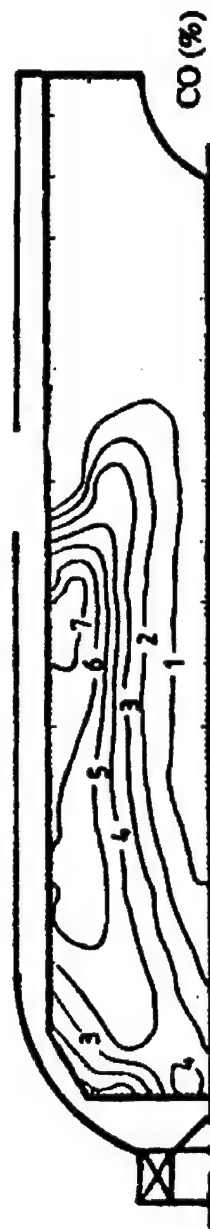


Figure 31b. Distribution of CO concentration in the mid-vertical plane (mole fraction, %).  
Test results.

LOCAL MX= 8.955  
 LOCAL MN= -.3729E-08

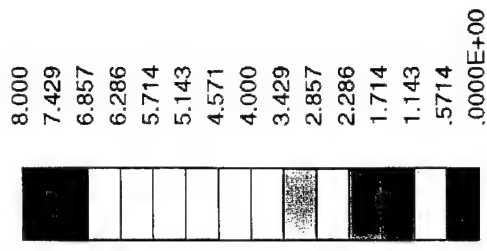


Figure 32a. Distribution of CO<sub>2</sub> concentration in the mid-horizontal plane (mole fraction, %).  
 CFD results.

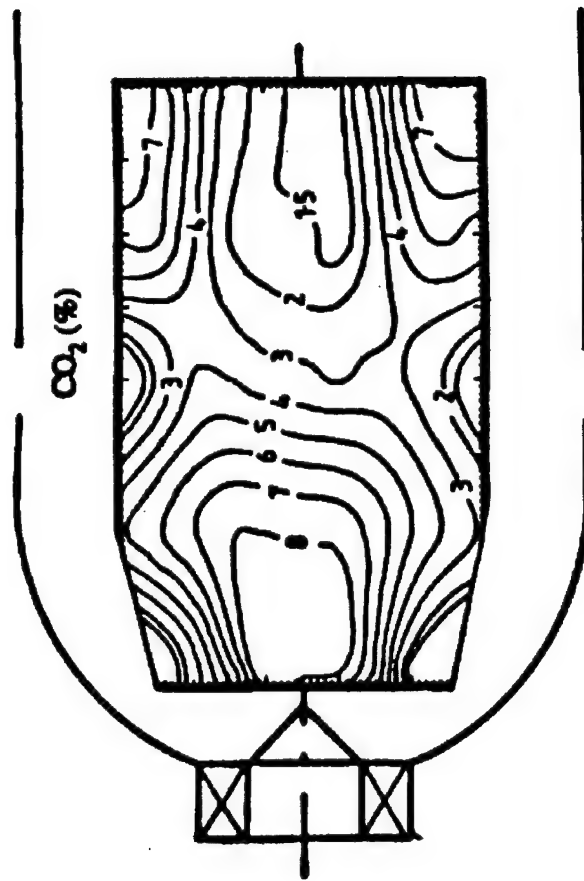


Figure 32b. Distribution of CO<sub>2</sub> concentration in the mid-horizontal plane (mole fraction, %).  
Test results.

LOCAL MX= 8.781  
 LOCAL MN= .0000E+00

8.000
7.429
6.857
6.286
5.714
5.143
4.571
4.000
3.429
2.857
2.286
1.714
1.143
.5714
.0000E+00



X  
 Y  
 Z

Figure 33a. Distribution of CO<sub>2</sub> concentration in the mid-vertical plane (mole fraction, %).  
 CFD results.



Figure 33b. Distribution of CO<sub>2</sub> concentration in the mid-vertical plane (mole fraction, %).  
Test results.

LOCAL MX= 15.98  
 LOCAL MN= -.4089E-08

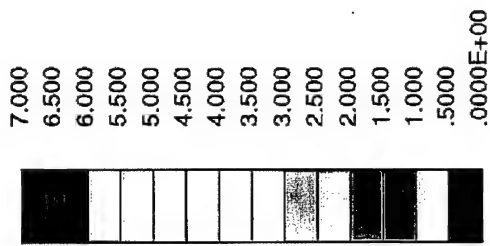


Figure 34a. Distribution of  $H_2$  concentration in the mid-horizontal plane (mole fraction, %).  
 CFD results.

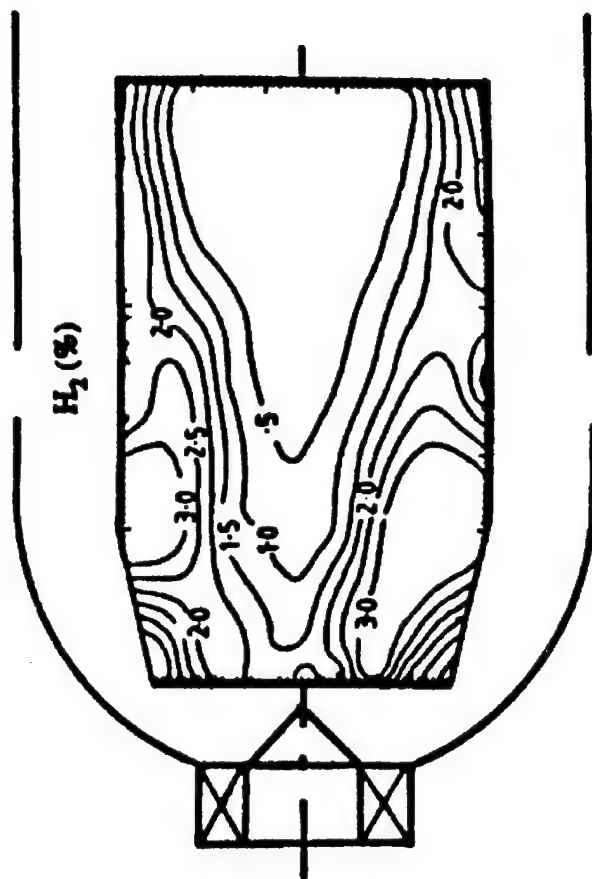


Figure 34b. Distribution of  $H_2$  concentration in the mid-horizontal plane (mole fraction, %).  
Test results.

LOCAL MX= 14.19  
 LOCAL MN= .0000E+00

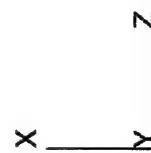
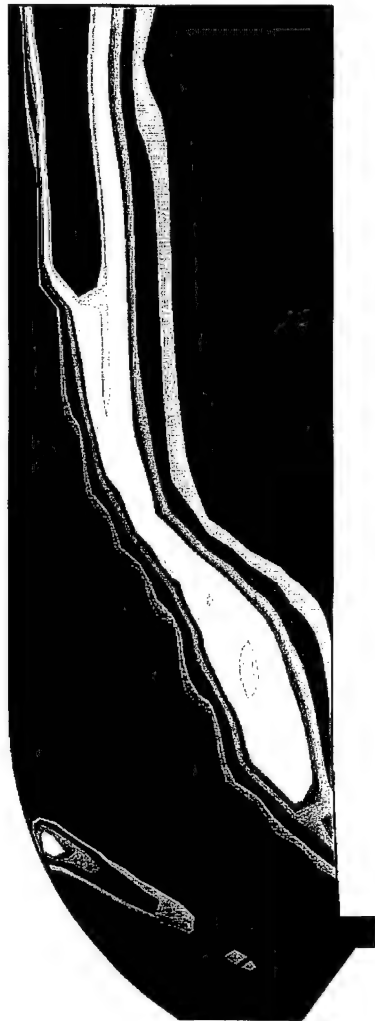
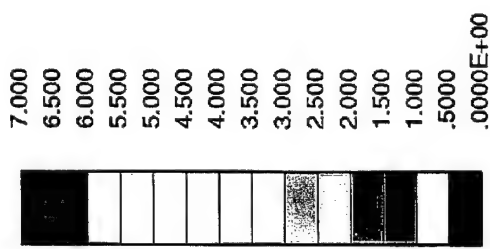


Figure 35a. Distribution of  $H_2$  concentration in the mid-vertical plane (mole fraction, %).  
 CFD results.

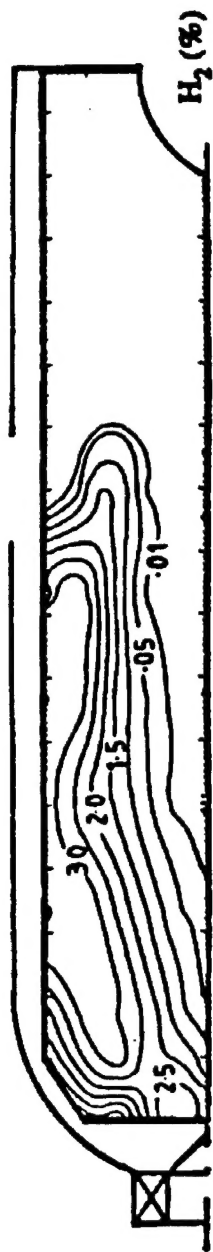


Figure 35b. Distribution of  $H_2$  concentration in the mid-vertical plane (mole fraction, %).  
Test results.

### Section 3

#### REFERENCES

- Bilger, R.W., "The Structure of Turbulent Non-Premixed Flames," Twenty-Second Symposium (International) on Combustion, The Combustion Institute, Pittsburgh, PA, pp. 475-488, 1988.
- Baulch, D.L., Cobos, C.J., Cox, R.A., Frank, P., Hayman, G., Just, Th., Kerr, J.A., Murrells, T., Pilling, M.J., Troe, J., Walker, R.W., Warnatz, J., "Summary Table of Evaluated Kinetic Data for Combustion Modeling," Comb. and Flame, 98, pp. 59-79, 1994.
- Bicen, A.F. and Jones, W.P., "Velocity Characteristics of Isothermal and Combusting Flows in a Model Combustor," Comb. Sci. and Tech., 49, pp. 1-15, 1986.
- Bicen, A.F., Tse, D.G.N., and Whitelaw, J.H., "Flow and Combustion Characteristics of an Annular Combustor," Comb. and Flame, 72, pp. 175-192, 1988.
- Bicen, A.F., Tse, D.G.N., and Whitelaw, J.H., "Combustion Characteristics of a Model Can-Type Combustor," Comb. and Flame, 80, pp. 111-125, 1990.
- Borisov, A.A., Dragalova, E.V., Zamanskii, V.M., Lisyanskii, V.V., and Skachkov, G.I., "Kinetics and Mechanism of Methane Self-Ignition," *Khim. Fizika*, N 4, pp. 536-543, 1982.
- Burcat, A. and McBride, B., "Ideal Gas Thermodynamic Data for Combustion and Air-Pollution Use," Technical Aerospace Engineering (TAE), Report # 804, 1997.
- Correa, S.M. and Shyy, W., "Computational Models and Methods for Continuous Gaseous Turbulent Combustion," Prog. En. and Comb. Sci., 13, pp. 249-292, 1987.
- Correa, S.M. and Gulati, A., "Measurements and Modeling of a Bluff-Body Stabilized Flame," Comb. and Flame, 89, pp. 195-213, 1992.
- Dagaut, P., Reuillon, M., Boettner, J.-C and Cathonnet, M., "Kerosene Combustion at Pressures up to 40 atm: Experimental Study and Detailed Chemical Kinetic Modeling," Twenty-Fifth Symposium (International) on Combustion, The Combustion Institute, Pittsburgh, PA, pp. 919-926, 1994.
- Dagaut, P., Reuillon, M., Boettner, J.-C and Cathonnet, M., "Chemical Kinetic Study of Dimethylether Oxidation in a Jet Stirred Reactor from 1 to 10 atm: Experiments and Kinetic Modeling," Twenty-Sixth Symposium (International) on Combustion, The Combustion Institute, Pittsburgh, PA, pp. 627-632, 1996.
- Gueret, C., Cathonnet, M., Boettner, J.-C., and Gaillard, F., "Experimental Study and Modeling of Kerosene Oxidation in a Jet-Stirred Flow Reactor," Twenty-Third Symposium (International) on Combustion, The Combustion Institute, Pittsburgh, PA, pp. 211-216, 1990.
- Heitor, M.V. and Whitelaw, J.H., "Velocity, Temperature, and Species Characteristics of the Flow in a Gas-Turbine Combustor," Comb. and Flame, 64, pp. 1-32, 1986.
- Konnov, A.A., "Detailed Reaction Mechanism for Small Hydrocarbons Combustion," Release 0.21, <http://homepages.vub.ac.be/~akonnov/>, 1997.
- Liew, S.K., Bray, K.N.C., and Moss, J.B., "A Stretched Laminar Flamelet Model of Tubulent Non-Premixed Combustion," Comb. and Flame, 56, pp. 199-213, 1984.
- Magnussen, B.F., Hjertager, B.H., Olsen, J.G., and Bhaduri, D., "Effects of Turbulent Structure and Local Concentrations on Soot Formation and Combustion in  $C_2H_2$  Diffusion Flames," Seventeenth Symposium (International) on Combustion, The Combustion Institute, Pittsburgh, PA, 1979, pp. 1383-1393.

Masri, A.R., Dibble, R.W., and Barlow, R.S., "Raman-Rayleigh Measurements in Bluff-Body Stabilised Flames of Hydrocarbon Fuels," Twenty-Fourth Symposium (International) on Combustion, The Combustion Institute, Pittsburgh, PA, 1992, pp. 317-324.

Masri, A.R., private communications, 1995.

Miller, J.A., and Bowman, C.T., "Mechanism and Modeling of Nitrogen Chemistry in Combustion," Prog. En. and Comb. Sci., 15, pp. 287-338, 1989.

Nandula, S.P., Pitz, R.W., Barlow, R.S., and Fiechtner, G.J., "Rayleigh/Raman/LIF Measurements in a Turbulent Lean Premixed Combustor," Paper AIAA 96-0937, 34<sup>th</sup> AIAA Aerospace Sciences Meeting, Reno, NV, January 15-18, 1996.

Peters, N., "Laminar Flamelet Concepts in Turbulent Combustion," Twenty-First Symposium (International) on Combustion, The Combustion Institute, Pittsburgh, PA, 1986, pp. 1231-1250.

Ranzi, E., Sogardo, A., Gaffuri, P., Pennati, G., and Faravelli, T., "A Wide Range Modelling Study of Methane Oxidation," Comb. Sci. and Tech., 96, pp. 279-325, 1994.

Tan, Y., Dagaut, P., Cathonnet, M., and Boettner, J.C., "Acetylene Oxidation in a JSR from 1 to 10 atm and Comprehensive Modelling," Comb. Sci. and Tech., 102, pp. 21-55., 1994.

Tolpadi, A.K., Hu, I.Z., Correa, S.M., and Burrus, D.L., "Coupled Lagrangian Monte Carlo PDF-CFD Computation of Gas-Turbine Combustor Flow Fields with Finite-Rate Chemistry," Paper ASME 96-GT-205, International Gas Turbine and Aeroengine Congress & Exhibition, Birmingham, UK, June 10-13, 1996.

Warnatz, J., "Rate Coefficients in the C/H/O System," *Combustion Chemistry*, W.C. Gardiner, Jr., Ed., Springer-Verlag, New York, 1984.

#### **Section 4**

### **WRITTEN PUBLICATIONS**

This report is not comprehensive in terms of the details of the work that was performed. Additional descriptions may be found in the several refereed reports that were produced as a result of this contract.

Refereed publications based on work performed in and written during the reporting period were:

1. Correa, S.M., "The Influence of Particle Count on IEM Monte Carlo Combustion Calculations," Paper AIAA 95-2439, 31<sup>st</sup> AIAA/ASME/SAE/ASEE Joint Propulsion Conference, San Diego, CA, July 10-12, 1995.
2. Tolpadi, A.K., Correa, S.M., Burrus, D.L., and Mongia, H.C., "A Monte Carlo PDF Method for the Calculation of Gas-Turbine Combustor Flow Fields," Paper AIAA 95-2443, 31<sup>st</sup> AIAA/ASME/SAE/ASEE Joint Propulsion Conference, San Diego, CA, July 10-12, 1995.
3. Tolpadi, A.K., Hu, I.Z., Correa, S.M., and Burrus, D.L., "Coupled Lagrangian Monte Carlo PDF-CFD Computation of Gas-Turbine Combustor Flow Fields with Finite-Rate Chemistry," Paper ASME 96-GT-205, International Gas Turbine and Aeroengine Congress & Exhibition, Birmingham, UK, June 10-13, 1996.
4. Hu, I.Z. and Correa, S.M., "Calculations of Turbulent Flames Using a PSR Microstructural Library," Twenty-Sixth International Symposium on Combustion, July 28 - August 2, 1996, Naples, Italy.
5. Correa, S.M., Hu, I.Z., and Tolpadi, A.T., "Combustion Technology for Low Emissions Gas-Turbines: Some Recent Modeling Results," ASME J. of Energy Resources Technology, Vol. 118, pp. 201-208, 1996.
6. Correa, S.M., Dean, A.J., and Hu, I.Z., "Combustion Technology for Low Emissions Gas-Turbines: Selected Phenomena Beyond  $\text{NO}_x$ ," ASME J. of Energy Resources Technology, 118, pp. 193-200, 1996.

#### **Section 5**

### **PROFESSIONAL PERSONNEL**

Dr. Sanjay M. Correa and Dr. Iris Z. Hu performed technical work on this program.

#### **Section 6**

### **INTERACTIONS/TECHNOLOGY TRANSFER**

Combustion and test facilities point of contact for NASA Lewis - GE "alliance." The purpose is to develop a non-duplicative development strategy for combustion, between NASA and all of GE. The activity was initiated by Dr. Carol Russo, Director of Aeronautics, at NASA Lewis. NASA's combustion point of contact is Dr. Valerie Lyons.

Monte Carlo methods and physical/chemical sub-models for aeroengine combustor design tools, e.g., the 3D CFD codes "CONCERT" and "ACC." David L. Burrus, at GE Aircraft Engines, Evendale, OH, (513) 243-2611 is the principal point of contact at GE Aircraft Engines.

#### **Section 7**

### **INVENTIONS**

There were no inventions in the reporting period.